

Liver-specific gene PGRMC1 blocks c-Myc-induced hepatocarcinogenesis through ER stress-independent PERK activation

Received: 7 March 2024

Accepted: 23 December 2024

Published online: 02 January 2025

 Check for updates

Fubo Ji^{1,2,3,9}, Jianjuan Zhang^{1,2,3,9}, Liping Mao^{1,2,3,9}, Yaqi Tan^{1,2,3}, Meihua Ye⁴, Xianglei He⁴, Yongzhi Zhao^{1,2,3}, Jiabin Liu^{1,2,3}, Yan Zhang^{1,2,3}, Nachuan Zhang^{1,2,3}, Jiong Shi⁵, Jianing Yan⁶, Xiujun Cai⁶, Bin Zhao⁶, Jianping Jin^{1,2,3}, Pinglong Xu^{1,3}, Stephanie Roessler⁷, Xin Zheng⁸ & Junfang Ji^{1,2,3,6} ✉

Roles of liver-specific genes (LSGs) in tumor initiation and progression are rarely explored in hepatocellular carcinoma (HCC). Here we show that LSGs are generally downregulated in HCC tumor tissues compared to non-HCC liver tissues, and low-LSG HCCs show poor prognosis and the activated c-Myc pathway. Among the c-Myc- and patient prognosis-associated LSGs, PGRMC1 significantly blocks c-Myc-induced orthotopic HCC formation. The role of PGRMC1 depends on its localization to the endoplasmic reticulum (ER) membrane, where PGRMC1 interacts with PERK through their ER luminal domains. This interaction in turn activates PERK in an ER stress-independent manner, which phosphorylates eIF2 α and consequently inhibits c-Myc protein translation. In HCC patients, PGRMC1 level is significantly reduced in tumor tissues and negatively associated with the c-Myc signature. Patients with low-PGRMC1 in their tumors have poor prognosis. Collectively, deregulated LSGs in HCC are associated with the c-Myc pathway activation and PGRMC1 blocks c-Myc-induced hepatic carcinogenesis through promoting ER stress-independent PERK activation.

Hepatocellular carcinoma (HCC) accounts for approximately 90% of all primary liver cancer, the fourth leading cause of cancer-related death worldwide¹. HCC is highly heterogeneous on many aspects such as various etiologies and various molecular subgroups based on HCC omics profiling^{2,3}. Among these HCC molecular subgroups, some were characterized by high levels of liver metabolism-related genes and/or liver function retention, and patients in these subgroups had relatively good prognosis^{4,5}. Liver-specific genes (LSGs) are a group of genes with specific high expression in liver compared to other human organs and

are related to liver metabolism functions. They are markers of hepatic terminal differentiation and are involved in hepatic basic and unique metabolism functions. LSGs were generally dysregulated in HCC tumors, while roles of LSGs in regulating HCC initiation and progression were rarely explored.

Progesterone receptor membrane component 1 (PGRMC1) was firstly found as a non-classic progesterone binding protein^{6,7}, which mediated progesterone anti-apoptosis function^{8,9}. It is a single-pass transmembrane protein with a carboxy-terminal cytochrome b5 heme-

¹The MOE Key Laboratory of Biosystems Homeostasis & Protection, Zhejiang Provincial Key Laboratory for Cancer Molecular Cell Biology, Life Sciences Institute, Zhejiang University, Hangzhou, Zhejiang 310058, China. ²Center for Life Sciences, Shaoxing Institute, Zhejiang University, Shaoxing, Zhejiang 321000, China. ³Cancer Center, Zhejiang University, Hangzhou, Zhejiang 310058, China. ⁴Zhejiang Provincial People's Hospital, Hangzhou, Zhejiang 310000, China. ⁵Department of Pathology, Nanjing Drum Tower Hospital, The Affiliated Hospital of Nanjing University Medical School, Nanjing, Jiangsu Province 210008, China. ⁶Department of General Surgery, Sir Run Run Shaw Hospital Affiliated to School of Medicine, Zhejiang University, Hangzhou, Zhejiang 310016, China. ⁷Institute of Pathology, University Hospital Heidelberg, Heidelberg 69120, Germany. ⁸Taoharmony Biotech L.L.C., Hangzhou, Zhejiang 310018, China. ⁹These authors contributed equally: Fubo Ji, Jianjuan Zhang, Liping Mao. ✉e-mail: junfangji@zju.edu.cn

binding domain¹⁰. Therefore, PGRMC1 could bind heme and regulate CYP450 enzymes^{11,12}. Except for its physiological function, roles of PGRMC1 in tumors remained largely undiscovered. In lung and breast cancers, PGRMC1 was upregulated and associated with tumor malignancy features^{13–15}. In HCC, its level was downregulated and patients with low PGRMC1 expression in their tumors had poor prognosis¹⁶. Meanwhile, PGRMC1 knockout (KO) mice were slightly more resistant to the development of HCC in the DEN-induced liver tumor mouse model¹⁷. Further investigation on PGRMC1 in cancer is thus required.

Protein kinase R (PKR)-like endoplasmic reticulum kinase (PERK) is a type I endoplasmic reticulum (ER) membrane protein. Its activation deactivates the eukaryotic initiation factor 2 α (eIF2 α) via phosphorylating eIF2 α at S51, consequently reducing protein translation¹⁸. PERK activation is mostly known in an ER stress-dependent manner. In the ER, BiP binds constitutively to the ER-luminal domains of PERK and sequesters it in an inactive form. When ER stress occurs, misfolded proteins accumulate and bind to BiP, which releases PERK from BiP interaction. Then, PERK homodimerizes or oligomerizes and trans-autophosphorylates to decline the protein synthesis via phosphorylating eIF2 α ^{18,19}. Recently, it was reported that PERK can also be activated at an ER stress-independent way. STING at the ER bound and directly activated the ER-located kinase PERK via their cytoplasmic domains²⁰. It was an intriguing question whether existing proteins activated PERK via their ER-luminal domains and in an ER stress-independent manner.

In the Human Protein Atlas (HPA, <https://www.proteinatlas.org/>), 759 LSGs are categorized with four-time higher mRNA expression in liver compared to any other tissues or the average level of all other tissues. We have previously found that CYP39A1, one of the LSGs, significantly suppressed HCC initiation and progression²¹. A liver-specific miRNA, miR-192-5p, was silenced in HCCs and significantly reduced HCC malignancy features^{22,23}. Given the natural high levels of LSGs in the liver and their potential roles in suppressing HCC, it is noteworthy to thoroughly investigate the roles of LSGs in hepatic carcinogenesis and progression.

In this work, we aim to systematically explore the relationship between these 759 LSGs and HCCs, and discover the key LSGs with roles in blocking HCC development and progression. Our results demonstrate that LSGs are heterogeneously expressed in HCC tumors and negatively associated with c-Myc signaling pathway. Meanwhile, PGRMC1, one of the key liver-specific gene, significantly blocks c-Myc-induced orthotopic HCC formation by inhibiting c-Myc protein translation via the PERK/p-eIF2 α axis.

Results

The expression level of LSGs were negatively associated with c-Myc signaling pathway

To assess the roles of LSGs in HCC, we analyzed the mRNA profiles of 759 LSGs in non-tumor and tumor tissues from 718 HCC patients in three independent cohorts (cohorts 1–3). The levels of these LSGs were mostly reduced in tumors compared to non-tumor liver tissues of HCC patients, and distinctively classified the samples to non-tumor and tumor tissues in all three cohorts (Fig. 1A, Supplementary Fig. 1A). Meanwhile, they also showed a heterogeneous expression pattern in HCC tissues. Based on their levels in tumor tissues, HCC patients were classified into high-, middle-, and low-LSG expression groups (Fig. 1B). HCC patients of high-LSG group tended to have significantly lower levels of alpha fetoprotein (AFP, a well-known HCC serum biomarker) as well as lower tumor grade and tumor stage (Fig. 1B and Supplementary Tables 1–3). Consistently, high-LSG patients had better overall survival compared to middle-LSG and low-LSG patients in cohorts 1–3 (Fig. 1C).

To examine the associated molecular signatures within patients of the high-LSG group, gene set enrichment analysis (GSEA) was performed. This resulted in 34 commonly enriched signatures in all three

cohorts. Among them, liver cell metabolism function signatures ($n = 22$) and HCC-related better prognosis signatures ($n = 9$) were significantly enriched in the high-LSG HCC subgroup (Fig. 1D). Moreover, the suppression of three oncogenic signaling pathways including two c-Myc pathways was also enriched (Fig. 1D).

MYC amplification is one of the most frequent genetic events in HCC²⁴. With well-established c-Myc target genes as we have used before²¹, HCC patients were subclassified respectively into strong, middle and weak c-Myc activation groups (Supplementary Fig. 1B). Significantly, HCC patients with weak c-Myc activation were enriched in the high-LSG subgroup while patients with strong c-Myc activation were in the low-LSG subgroup (Fig. 1E, $P < 0.001$ for each cohort). Vice versa, high-LSG patients were enriched in the HCC subgroup with weak c-Myc activation while low-LSG patients were in strong c-Myc activation subgroup (Fig. 1F, $P < 0.001$ for each cohort).

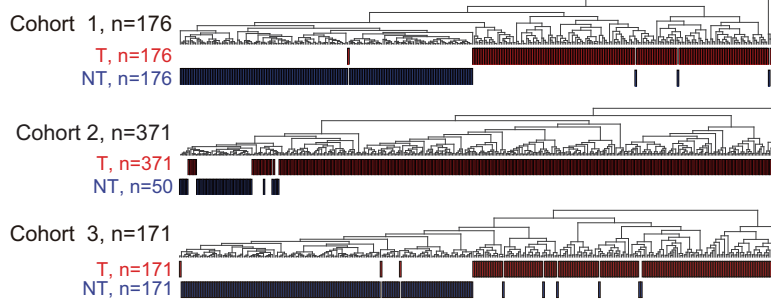
To examine whether such a negative relationship between LSGs and c-Myc activation was caused by c-Myc targets among LSGs, LSGs were further divided into potential Myc-targeted LSGs ($n = 165$) and non Myc-targeted LSGs ($n = 594$) based on Myc Chip-seq data in HepG2 cells^{25,26} (Supplementary Fig. 2A). Regardless of the patient grouping based on Myc-targeted LSGs or non-Myc-targeted LSGs, patients with strong c-Myc activation always gathered in the low-LSG subgroups, while patients with weak c-Myc activation were in the high-LSG subgroups across three cohorts (Supplementary Fig. 2B, C, $P < 0.001$ for each enrichment). Together, LSGs were heterogeneously expressed in HCCs, and their expression levels were negatively associated with c-Myc activation status, even when considering non Myc-targeted LSGs.

LSG PGRMC1 significantly suppressed c-Myc-induced HCC

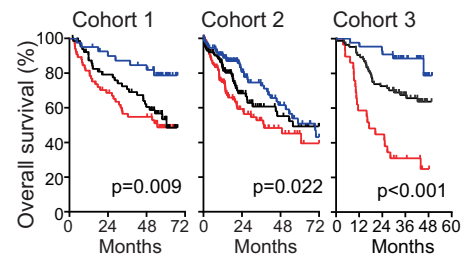
Given the negative correlation between non Myc-targeted LSGs and the activated c-Myc signaling, one possibility was that some LSGs might be the suppressor of c-Myc signaling pathway. We screened LSGs negatively associated with c-Myc activation and patient prognosis, and then evaluated their tumor suppressor roles using the Myc/Mcl1-induced hydrodynamic tail vein injection (HDTV) HCC mouse model. In cohorts 1 and 2, 40 LSGs were expressed differentially between the strong c-Myc activation subgroup and the weak c-Myc activation subgroup ($P < 0.001$), and related to HCC prognosis ($P < 0.05$) (Fig. 2A, B). Among them, the top five c-Myc related LSGs (ABAT, FMO4, HAGH, PGRMC1 and SLC10A1) were further evaluated in cohort 3 and consistent data were obtained (Fig. 2B). In Myc/Mcl1-induced HDTV HCC model with ICR mouse strain, three out of five LSGs significantly inhibited c-Myc-induced HCC formation and prolonged mouse survival, with PGRMC1 showing the strongest inhibitory ability (Fig. 2C, D). Specifically, all mice in the control group ($n = 6$) had to be killed due to HCC tumor burden, whereas all mice in the PGRMC1 group ($n = 6$) were alive and 60% of mice (4 out of 6) had no tumor formation (Fig. 2D).

The ability of the LSG PGRMC1 in suppressing c-Myc-induced HCC was further confirmed in Myc/Mcl1-induced HCC model with FVB mouse strain (Fig. 2E). Briefly, the delivered PGRMC1 was overexpressed in mouse liver (Supplementary Fig. 3A). At 5.5 weeks after HDTV all mice developed liver tumors in the control group, while only 42.9% of mice developed tumors in the PGRMC1 group. PGRMC1 also significantly reduced Myc/Mcl1-mediated tumor burden, shown by significantly decreased liver/body ratios, tumor numbers and tumor sizes. Moreover, the HCC mouse model induced with c-Myc alone was used to avoid the potential effects of Mcl1 in FVB mice, and comparable data were obtained (Fig. 2F). At 9.5 weeks after HDTV, 87.5% of mice developed liver tumors in the control group while only 16.7% (one out of six) mice developed one small tumor nodule in the PGRMC1 group. Thus, across three mouse models, PGRMC1 significantly reduced c-Myc-mediated HCC tumor burden. Furthermore, we also reduced the PGRMC1 dose in Myc/

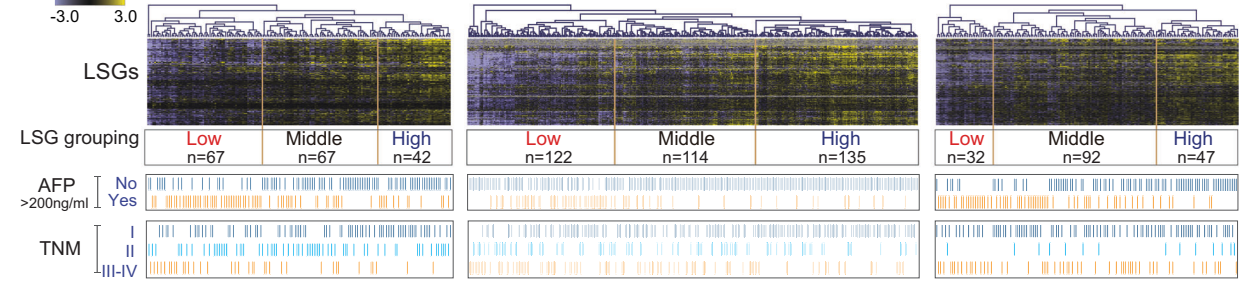
A Clustering based on LSG genes



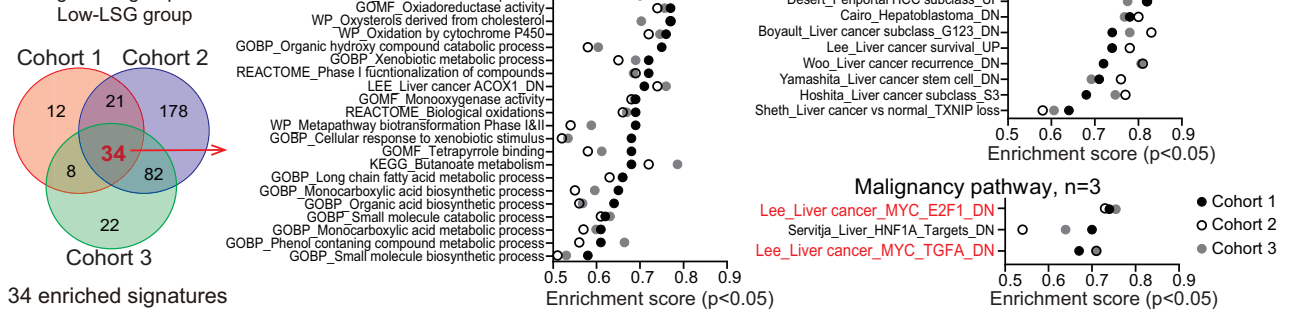
C LSG grouping



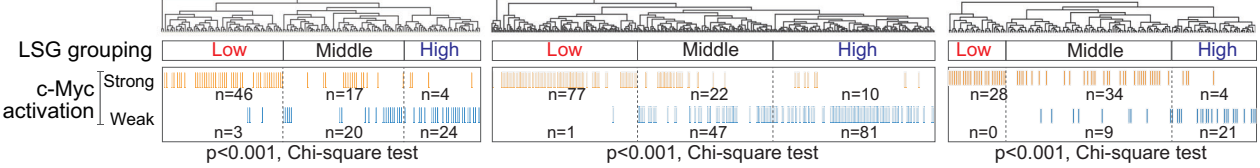
B Cohort 1, tumor



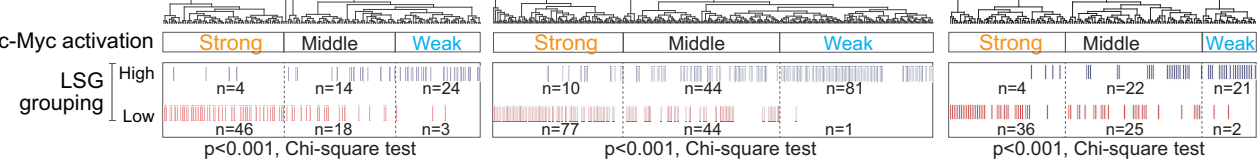
D GSEA analysis



E



F



Mcl1-induced HCC model to one third of PGRMC1 that we used in Fig. 2E. A significant HCC suppression was also consistently obtained (Supplementary Fig. 3B).

We further examined whether PGRMC1 suppressed tumor burden after HCC had developed using the Myc/Mcl1 HCC mouse model and the packaged AAV8.PGRMC1. Luciferase plasmid was co-injected with Myc/Mcl1 to assess the tumor burden by bioluminescence imaging

(Fig. 2G). AAV particles were delivered at 3 weeks after oncogene injection. AAV8.PGRMC1 (Supplementary Fig. 4) significantly inhibited tumor growth over time shown by the reduced luminescence in liver (Fig. 2G, H), and prolonged mouse overall survival with a medium survival increasing from 9 to 14 weeks (Fig. 2H). Collectively, the liver-specific gene PGRMC1 significantly inhibited c-Myc-induced HCC formation and progression.

Fig. 1 | LSGs were heterogeneously expressed in HCC and associated with c-Myc signaling. **A** In cohorts 1-3, HCC patients were clustered by liver-specific genes expression in non-tumor and tumor tissues. NT non-tumor. T tumor. **B** HCC patients were divided into low-, middle- and high- LSGs expression groups, clustered by LSG levels in tumor tissues. The number of cases were indicated. The status of AFP level and TNM stage for each patient were labeled. **C** Kaplan-Meier analysis of time to recurrence and overall survival for three groups of HCC cases in cohorts 1-3. Log-rank test was performed. **D** In cohorts 1-3, GSEA analysis were performed between HCC patients with high LSG levels and ones with low LSG levels

in their tumors. Venn diagram analysis revealed the 34 signatures in LSG high group which were commonly enriched in three independent cohorts. Enrichment score (ES) is computed using a weighted Kolmogorov-Smirnov test and signature with the nominal p -value of ES score <0.05 is shown (one-sided). **E** In cohorts 1-3, c-Myc activation status in low-, middle- and high- LSG expression HCC subgroups. **F** LSG expression status in strong, middle, and weak c-Myc activation HCC subgroups in cohort 1-3. **E, F** The number of cases in each group or subgroup was indicated in the figure. Chi-square test was performed (two-sided). Source data are provided as a Source Data file.

LSG PGRMC1 was heterogeneously expressed in HCC tumors and its low level was associated with malignant features of HCC patients

The liver-specific expression of PGRMC1 was firstly confirmed. Among 20 normal human organs, human liver exhibited the highest expression level of PGRMC1 (Fig. 3A). In NCBI RNA sequencing data of human and mouse organs, PGRMC1 also showed the highest expression in adult liver (Supplementary Fig. 5A).

In HCC cohorts 1-3, PGRMC1 mRNA levels in HCC tumor were more heterogenous than non-HCC liver tissues (Figs. 2B and 3B, Supplementary Fig. 5B) and generally downregulated in HCCs compared to non-HCC liver tissues (Fig. 3B, $P < 0.001$ in cohorts 2-3, $P = 0.30$ in cohort 1). Noticeably, it was significantly down-regulated in HCC tumors compared to non-tumors from the strong c-Myc activation HCC subgroup ($P < 0.001$ for all three cohorts), but not in HCC tumors from weak c-Myc activation HCC subgroup in all three cohorts (Supplementary Fig. 5C).

Consistent data were obtained for PGRMC1 protein. In proteomics data of cohort 3, PGRMC1 was significantly downregulated in tumor tissues compared to non-tumor liver tissues (Fig. 3C). In 7 out of 10 paired tumor and non-tumor tissues from HCC patients of cohort 4, PGRMC1 showed a reduced protein level in HCC tumor tissues compared to the paired non-tumor liver tissues via western blot assay (Fig. 3D). PGRMC1 immunohistochemistry (IHC) analysis was also performed in a tissue array including 328 FFPE samples from HCC patients (cohort 5). Consistently, PGRMC1 exhibited a heterogenous expression in HCC tumors and a lower level in tumor compared to non-HCC liver tissue (Fig. 3E, $P < 0.001$). In addition, both mRNA and protein expression of PGRMC1 were downregulated in c-Myc-induced mouse liver tumor tissues compared to non-tumor liver tissues (Supplementary Fig. 5D, E).

Furthermore, HCC patients with lower PGRMC1 levels showed higher serum AFP level and worse differentiation grades in their tumors in cohort 5 (Supplementary Table 4). Comparably, PGRMC1 level was significantly lower in HCC patients with AFP > 200 ng/ml than ones with AFP ≤ 200 ng/ml (Fig. 3F), and gradually reduced in HCC tumors from well differentiated status to poorly differentiated status (Fig. 3G). Meanwhile, patients with low PGRMC1 protein level in their tumors also exhibited worse survival than PGRMC1-high patients based on the PGRMC1 median cut-off in cohort 5 (Fig. 3H). Consistent data were obtained in cohorts 1-3 (Fig. 3I, J, Fig. 2B, Supplementary Tables 5-7). Together, the LSG PGRMC1 was heterogeneously expressed in HCC tumor tissues and HCC patients with low level of PGRMC1 had worse prognosis.

PGRMC1 reduced c-Myc protein level by inhibiting its protein translation

The mechanism of PGRMC1 was then investigated in suppressing c-Myc-induced HCC. In HCC cells, silencing PGRMC1 increased endogenous c-Myc protein level (Fig. 4A, Supplementary Fig. 6A), while silencing c-Myc did not affect PGRMC1 protein expression (Supplementary Fig. 6B). Consistently, PGRMC1 overexpression significantly reduced both endogenous and exogenous c-Myc protein level in HCC cells (Fig. 4B, C). Comparable data were also noticed in Myc/Mcl-1 induced HCC mouse model (Supplementary

Fig. 6C). However, PGRMC1 did not alter c-Myc mRNA expression (Fig. 4A, B) or its protein stability (Supplementary Fig. 6D, E). The reduction of c-Myc protein level mediated by PGRMC1 could not be rescued either by MG132, a proteasome-related degradation inhibitor, or by BafA1, a lysosome-related degradation inhibitor (Supplementary Fig. 6F, G). In addition, PGRMC1 did not interact with c-Myc either (Supplementary Fig. 6H).

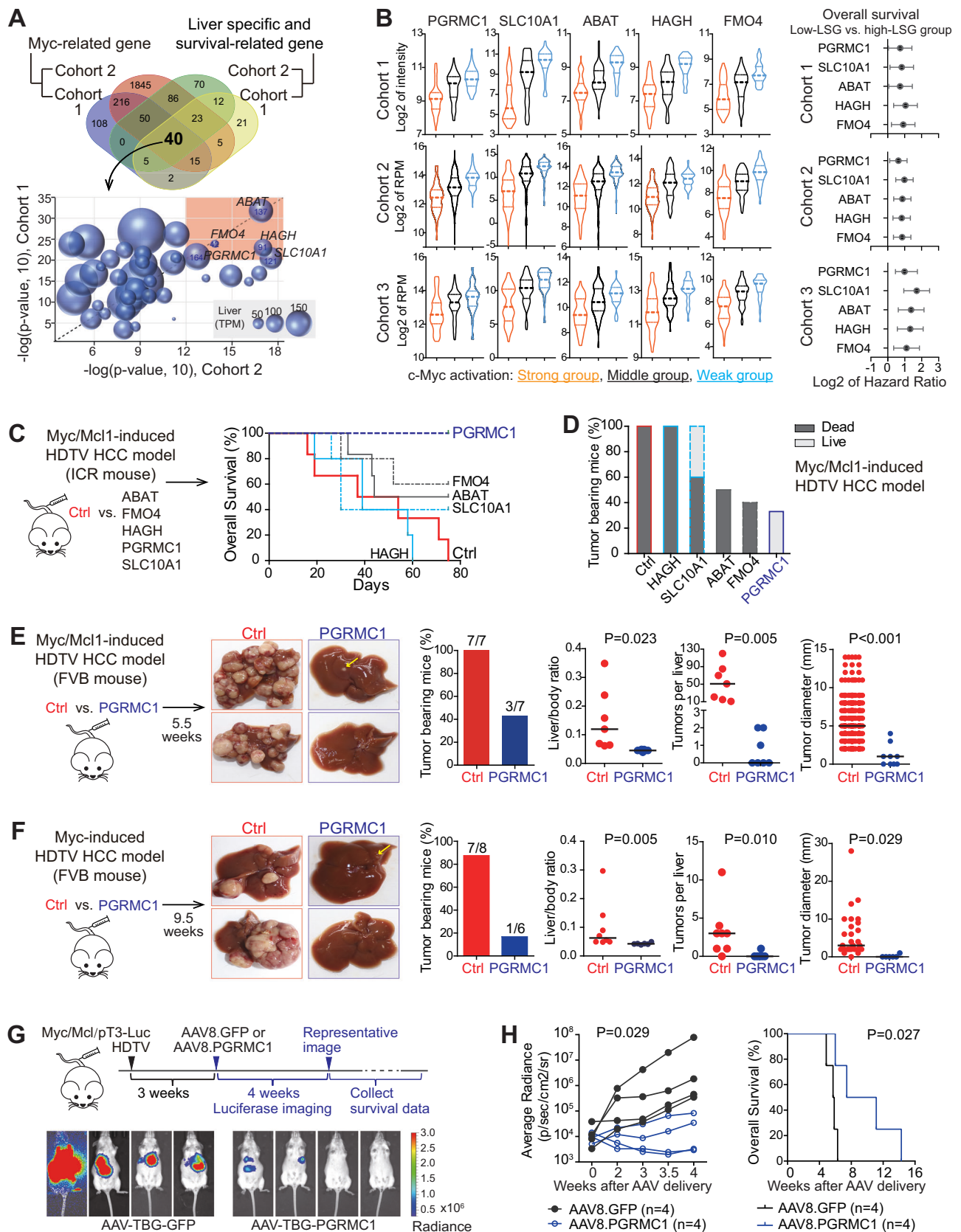
In this case, we tested whether PGRMC1 interfered c-Myc protein translation using Boncat assay, which allowed the detection of newly synthesized proteins^{27,28}. In both Huh7 and Huh1 cells, overexpressed PGRMC1 significantly suppressed the protein synthesis of exogenous c-Myc (Fig. 4D). Comparable data were obtained for endogenous c-Myc (Fig. 4E). Vice versa, silencing PGRMC1 increased c-Myc protein translation in both Huh7 and Huh1 cells (Fig. 4F). Collectively, PGRMC1 reduced c-Myc protein level via suppressing its protein translation.

PGRMC1 inhibited c-Myc protein translation via activating the PERK/p-eIF2 α axis

PGRMC1 mainly locates on the ER²⁹ (Supplementary Fig. 7), where the ER membrane protein PERK/ phosphorylated eIF2 α (p-eIF2 α) axis is responsible for protein synthesis suppression³⁰. Noticeably, when PERK was silenced with siRNAs in HCC cells, the PGRMC1-mediated c-Myc reduction was rescued (Fig. 5A, Supplementary Fig. 8A). Comparable data were obtained when HCC cells were exposed to PERK inhibitors iPERK-1 and iPERK-2 (Fig. 5B). Meanwhile, upon the silencing of PGRMC1 in HCC cells, p-eIF2 α level was suppressed regardless of the treatment of tunicamycin, an ER stress inducer (Fig. 5C). Moreover, the overexpressed PGRMC1 increased the p-eIF2 α level, while such an increase was canceled when PERK was either silenced (Fig. 5D) or suppressed (Fig. 5E). Thus, the PERK/p-eIF2 α axis was important in the PGRMC1-mediated c-Myc protein down-regulation.

PERK is one of the four eIF2 α kinases (EIF2AKs) and it is also named EIF2AK3. We then examined the role of the other three EIF2AKs, EIF2AK1 (HRI), EIF2AK2 (PKR), and EIF2AK4 (GCN2)³¹, in regulating PGRMC1-mediated c-Myc protein down-regulation. As shown in Supplementary Fig. 8B, C, PGRMC1 reduced the c-Myc protein level, which was not rescued upon silencing of these three EIF2AKs in HCC cells. These results suggested the specific role of PERK in PGRMC1-mediated c-Myc protein down-regulation. Moreover, with an available anti-mouse phospho-Perk antibody, we also found that PGRMC1 promoted phosphorylation of endogenous Perk in two mouse cell lines, i.e., 3T3 and Hepa1-6 cells (Fig. 5F). Comparably, silencing mouse Pgrmc1 (mPgrmc1) also noticeably reduced the phosphorylation of endogenous Perk in both cell lines (Supplementary Fig. 9).

Consistent data were obtained in vivo. Silencing PERK terminated the ability of PGRMC1 in suppressing c-Myc-induced tumor formation and tumor burden in the orthotopic HCC mouse model. Specifically, in the Myc/Mcl1 driven HCC mouse model, PGRMC1 significantly inhibited liver tumor formation and tumor burden. When PERK was silenced with two different shRNAs (Supplementary Fig. 10), the tumor suppression mediated by PGRMC1 was abolished. This was shown by the tumor incidence rate, liver/body ratios, tumor numbers and tumor sizes (Fig. 5G).



PGRMC1 interacted with PERK via their ER luminal domains, leading to PERK activation

To investigate how PGRMC1 activated PERK, co-immunoprecipitation (co-IP) was performed and an interaction was detected between exogenous PGRMC1 and PERK, as well as between endogenous PGRMC1

and PERK (Fig. 6A, Supplementary Fig. 11). In this case, the interaction domain of PGRMC1 and PERK was mapped by a series of co-IP assays. As shown in Fig. 6B, PGRMC1 strongly interacted with the ER-luminal domain of PERK (N-PERK) but not its cytosolic domain (C-PERK). Meanwhile, when PGRMC1 lost either its N-terminal region of 1-24aa

Fig. 2 | Liver-specific gene PGRMC1 significantly suppressed c-Myc-induced HCC tumor formation. **A** Venn diagram analysis of c-Myc- and survival-related LSGs in cohorts 1-2. c-Myc related genes were screened by class comparison of tumor tissue mRNA profiling between strong and weak c-Myc activation subgroups ($P < 0.001$, |fold change| > 2). Survival-related LSGs were screened by Kaplan-Meier survival analysis with a median cut-off of each LSG ($P < 0.05$). 40 c-Myc/survival-related LSGs were identified and shown by their P -values of c-Myc-related gene analysis. TPM, transcripts per million, from the average of three transcriptomics datasets (HPA, GTEx and FANTOM5). **B** Expression levels of the top 5 c-Myc/survival-related LSGs in different c-Myc activation groups (left panel, median and quartiles were shown), and their hazard ratio of low-LSG group survival vs. high-LSG group (right panel, hazard ratio with 95% confidence interval). For strong, middle and weak c-Myc activation groups, $n = 67, 62, 47$ in Cohort 1; $n = 109, 133, 129$ in Cohort 2; $n = 66, 75, 30$ in Cohort 3. **C** Screening LSGs in suppressing c-Myc-mediated HCC development with Myc/Mcl1-induced HDTV mouse model. Overall survival analysis was presented. Five to six mice for each group were used (Control,

ABAT, FMO4 and PGRMC1 groups, $n = 6$; HAGH and SLC10A1 groups, $n = 5$). **D** Tumor bearing mice (including mice died from tumor burden) in five LSG groups and the control group of Myc/Mcl1 mouse model. **E** Tumor formation in Myc/Mcl1-induced HCC mouse model with or without PGRMC1 overexpression. Control group, $n = 7$. PGRMC1 group, $n = 6$. **F** Tumor formation in c-Myc-induced HCC mouse model with or without PGRMC1 overexpression. Control group, $n = 8$. PGRMC1 group, $n = 6$. **E, F** Representative images were shown. Tumor bearing animals, liver/body ratio, tumors per liver, and tumor diameter were also quantified and compared. Student's t -test was performed (two-tailed). **G** Overall flow of Myc/Mcl1/luciferase-induced HCC mouse model treated with AAV8 particle. Representative images of in vivo bioluminescence imaging with mice treated with AAV8 at day 28 of post-injection. **H** Average bioluminescence radiance at 14, 21, 24, and 28 days after injecting AAV8 particle (4 mice per group). Two-way ANOVA was performed. Overall survival was shown for mice treated with AAV8.GFP or AAV8.PGRMC1 and Log-rank test was performed. Source data are provided as a Source Data file.

(PGRMC1^{Δ1-24}) or its transmembrane domain (PGRMC1^{Δ25-43}), the interaction of N-PERK with PGRMC1 was largely reduced (Fig. 6C). Thus, PGRMC1 interacted with PERK via their ER luminal domains. Consistently, PGRMC1 missing the PERK interaction domain could not activate the PERK/p-eIF2α axis in both mouse and human cells as the full-length PGRMC1 did (Supplementary Fig. 12).

PERK is usually present in an inactive form due to BiP binding constitutively to PERK ER-luminal domain. Noticeably, PGRMC1 reduced the interaction of PERK and BiP in both 293T cell line and HCC cell line Huh7 (Fig. 6D). Moreover, either PGRMC1^{Δ25-43} or PGRMC1^{Δ1-24}, losing the domains interacting with PERK, could not suppress the interaction of PERK and BiP as PGRMC1^{WT} did (Fig. 6E). We then tested whether the PGRMC1-mediated PERK/p-eIF2α activation was dependent on ER stress. In this case, two well-defined ER stress inhibitors, tauroursodeoxycholic acid (TUDCA) and 4-phenylbutyric acid (4-PBA) were used³²⁻³⁴. Both TUDCA and 4-PBA significantly reduced ER stress-induced p-eIF2α level (Supplementary Fig. 13). However, they did not reduce the PGRMC1-mediated eIF2α phosphorylation or rescue the PGRMC1-mediated reduction of exogenous c-Myc protein level (Fig. 6F). Comparably, PGRMC1-mediated reduction of endogenous c-Myc protein was not rescued by these ER stress inhibitors either (Fig. 6G). Consistent data were also obtained when ER stress inducer was used. The ER stress-mediated eIF2α phosphorylation was reduced upon silencing PGRMC1 (Fig. 5C). In addition, there are three known ER stress sensors, i.e., PERK, inositol requiring enzyme 1 (IRE1α), and the activating transcription factor 6 (ATF6). As shown in Supplementary Fig. 14, PGRMC1 did not seem to activate the other two ER stress sensors and their corresponding down-stream actors, i.e., IRE1α/spliced XBP1 (XBPs) and ATF6/BiP, but only activated PERK/p-eIF2α. Thus, PGRMC1 mediated the PERK/p-eIF2α activation at an ER stress-independent manner. Taken together, PGRMC1 N-terminus and its transmembrane domain were important for PGRMC1 to interact with PERK at the ER lumen, which disassociated PERK from BiP and consequently activated PERK in an ER stress-independent manner. This model is illustrated in Fig. 6H.

Both PGRMC1's ER localization and its N-terminus were important in inhibiting c-Myc translation and c-Myc-induced liver tumor formation

Consistent with the model, the immunofluorescence showed that the transmembrane domain of PGRMC1 was essential for its ER localization (Fig. 7A). Both PGRMC1^{WT} and PGRMC1^{Δ1-24} were clearly co-localized with the ER marker calreticulin near around nucleus, while PGRMC1^{Δ25-43} lost its co-localization with calreticulin and mainly located in cell nucleus. Meanwhile, PGRMC1 N-terminus interacted with PERK at its ER luminal region, indicating an ER lumen location of PGRMC1 N-terminus. This aligns with several reports on PGRMC1 N-terminus as its ER luminal region^{29,35,36}.

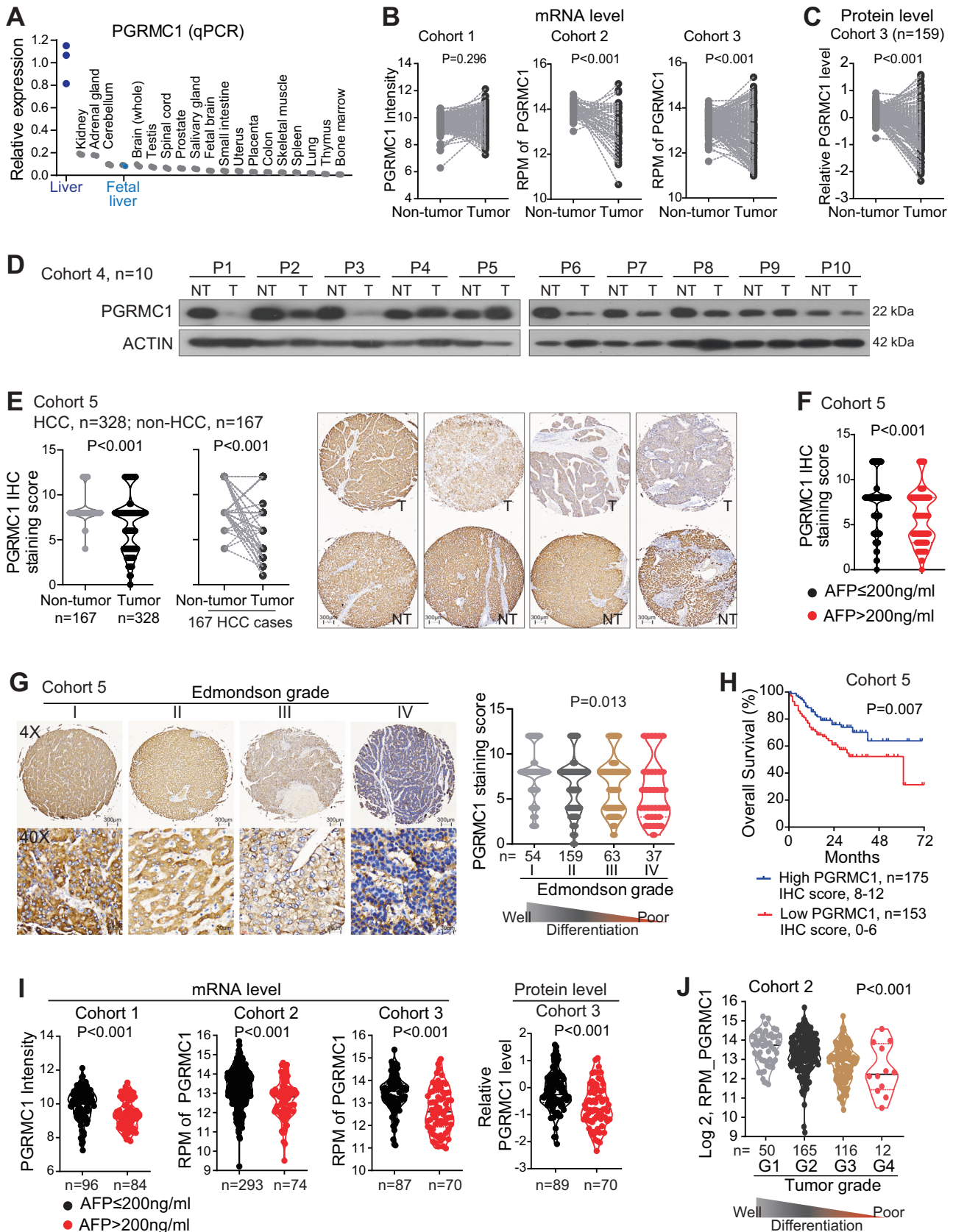
We then tested the importance of PGRMC1's ER localization and its luminal domain in suppressing c-Myc translation and c-Myc-induced HCC formation. As shown in Fig. 7B, C, PGRMC1^{Δ25-43} without ER localization no longer suppressed the protein translation of exogenous and endogenous c-Myc. In HCC mouse model, PGRMC1^{WT} significantly inhibited liver tumors formation and tumor burden, whereas PGRMC1^{Δ25-43} did not at all (Fig. 7D). Specifically, all mice developed liver tumors in control group and 66.7% of mice developed tumors in PGRMC1 group. However, all mice had tumors in PGRMC1^{Δ25-43} group. Meanwhile, PGRMC1^{Δ25-43} did not reduce c-Myc-mediated tumor burden, shown by liver/body ratios, tumor numbers and tumor sizes, as PGRMC1 did. Moreover, PGRMC1^{Δ1-24}, without PGRMC1 ER luminal domain, was not able to suppress the protein translation of both exogenous and endogenous c-Myc either (Fig. 7E, F). In orthotopic HCC mouse model, the tumor suppressor role of PGRMC1^{Δ2-24} was also significantly weaker than PGRMC1^{WT} (Fig. 7G). It was shown by an increased tumor formation rate, higher liver body ratio, higher tumor numbers and larger tumor sizes in the PGRMC1^{Δ2-24} group compared to the PGRMC1^{WT} group. Together, both the ER localization of PGRMC1 and its ER luminal domain were important for inhibiting c-Myc translation and c-Myc-mediated tumor formation.

A mini PGRMC1 (PGRMC1^{1-47aa}) was sufficient in activating PERK and suppressing Myc/Mcl1-induced tumor formation

To further elucidate the role of PGRMC1 in the PERK/c-Myc axis, we constructed a mini PGRMC1 only including its N-terminus and transmembrane domain, i.e., PGRMC1^{1-47aa} (Fig. 8A). Similar with PGRMC1^{WT}, PGRMC1^{1-47aa} co-localized with the ER marker calreticulin (Fig. 8B) and interacted with N-PERK (Fig. 8C). Meanwhile, PGRMC1^{1-47aa} also suppressed the interaction of PERK with BiP (Fig. 8D), and sufficiently suppressed exogenous c-Myc protein level and its protein translation (Fig. 8E). Comparable data were obtained for endogenous c-Myc (Fig. 8F). PGRMC1^{Δ25-43} was included as a negative control in Fig. 8C-F.

Consistent data were also noticed in vivo for the mini PGRMC1. In the Myc/Mcl1 driven HCC mouse model, PGRMC1^{1-47aa} significantly suppressed liver tumor formation and reduced tumor burden to a similar extent as PGRMC1^{WT} (Fig. 8G). All mice developed liver tumors in the control group, while 57.1% and 75% of mice developed tumors in PGRMC1^{WT} group and PGRMC1^{1-47aa} group, respectively. Moreover, both PGRMC1^{WT} and PGRMC1^{1-47aa} significantly reduced c-Myc-mediated tumor burden, shown by decreased liver/body ratios, tumor numbers and tumor sizes. No significant difference was obtained between PGRMC1^{WT} and PGRMC1^{1-47aa} groups.

PGRMC1^{1-47aa} also functioned in Myc/Mcl1 HCC mouse model after HCC has occurred. In this mouse model, AAV particles were delivered at 3 weeks after Myc/Mcl1 oncogene injection as we did in Fig. 2, when tumors have been developed (Fig. 8H). Consistent with the function of wild-type PGRMC1, AAV8.PGRMC1^{1-47aa} (Supplementary Fig. 15)



significantly prolonged mouse overall survival compared to the control AAV8 group ($p = 0.009$, Fig. 8H). Collectively, PGRMC1^{L-47aa} activated PERK and effectively suppressed Myc/Mcl1-induced tumor formation in vivo.

Discussion

LSGs are markers of hepatic terminal differentiation and vital for the basic and unique liver metabolism function. Our recent studies showed that CYP39A1 as a LSG remarkably suppressed HCC

Fig. 3 | PGRMC1 was downregulated in HCC tumor tissues, especially in those tissues with poorly differentiation. **A** PGRMC1 expression in 20 normal human organs by RT-qPCR. These RNAs were commercially available and each organ RNA was a pooled RNA which was originally from more than three different individuals. Data were from three technique triplicates of the pooled RNAs. **B** PGRMC1 mRNA levels in paired non-tumor and tumor tissues of HCC patients from cohorts 1-3. **C** PGRMC1 protein levels in paired non-tumor and tumor tissues of HCC patients from cohort 3. **D** PGRMC1 protein level was detected by Western Blot in paired non-tumor and tumor tissues of HCC patients from cohort 4. **E** PGRMC1 IHC staining in cohort 5. The quantitative data and representative images were shown. Scale bar, 300 μ m. **F** PGRMC1 levels in HCC tumors from AFP positive (> 200 ng/ml, $n = 90$) or

AFP negative (≤ 200 ng/ml, $n = 166$) HCC patients in cohort 5. **G** Representative images and quantitative data of PGRMC1 staining in HCC tumor with different Edmondson grades in HCC cohort 5. Scale bars, 300 μ m for the top panel and 30 μ m for the bottom panel. **H** Kaplan-Meier analysis of overall survival in HCC cases from cohort 5 based on PGRMC1 protein level. Log-rank test was performed. **I** PGRMC1 levels in HCC tumors from AFP positive or AFP negative HCC patients in cohorts 1-3. The number of cases were indicated. **J** PGRMC1 levels in tumors with different tumor grades in cohort 2. **B, C, F, I** Student's *t*-test was performed (two tailed). **E** Non-parametric *t*-test was performed (two-tailed). **G, J** One-way ANOVA was performed. Source data are provided as a Source Data file.

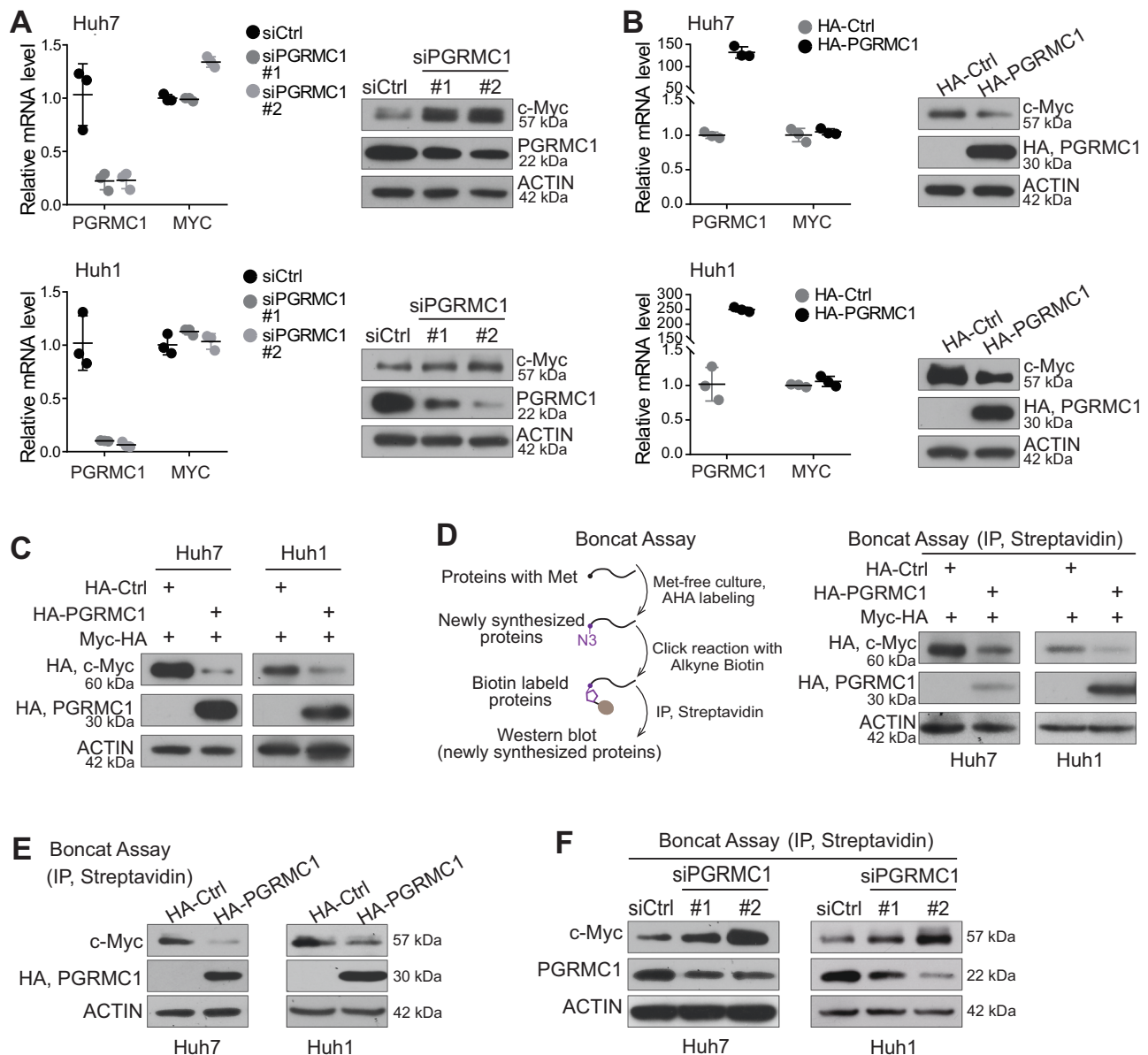
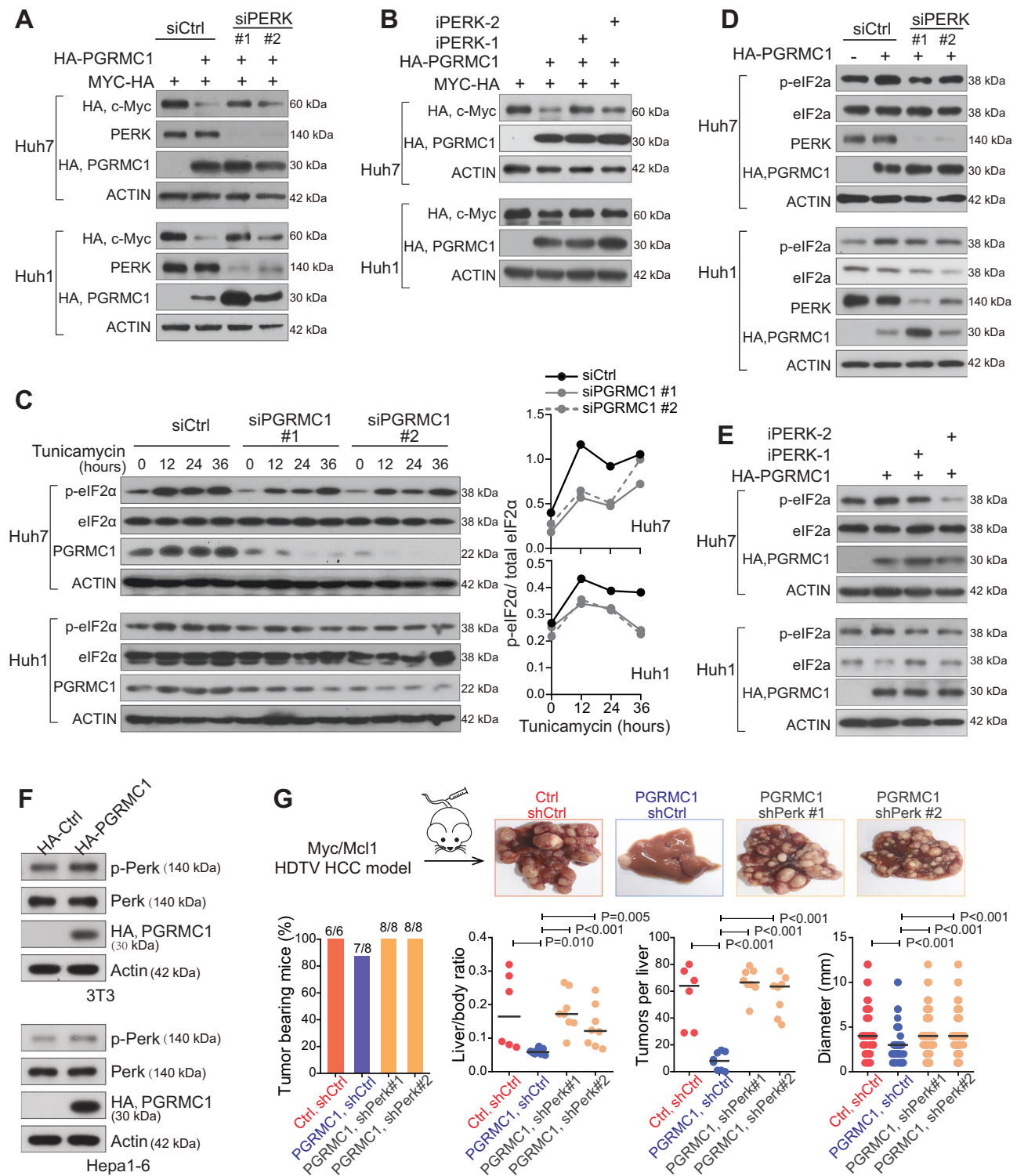
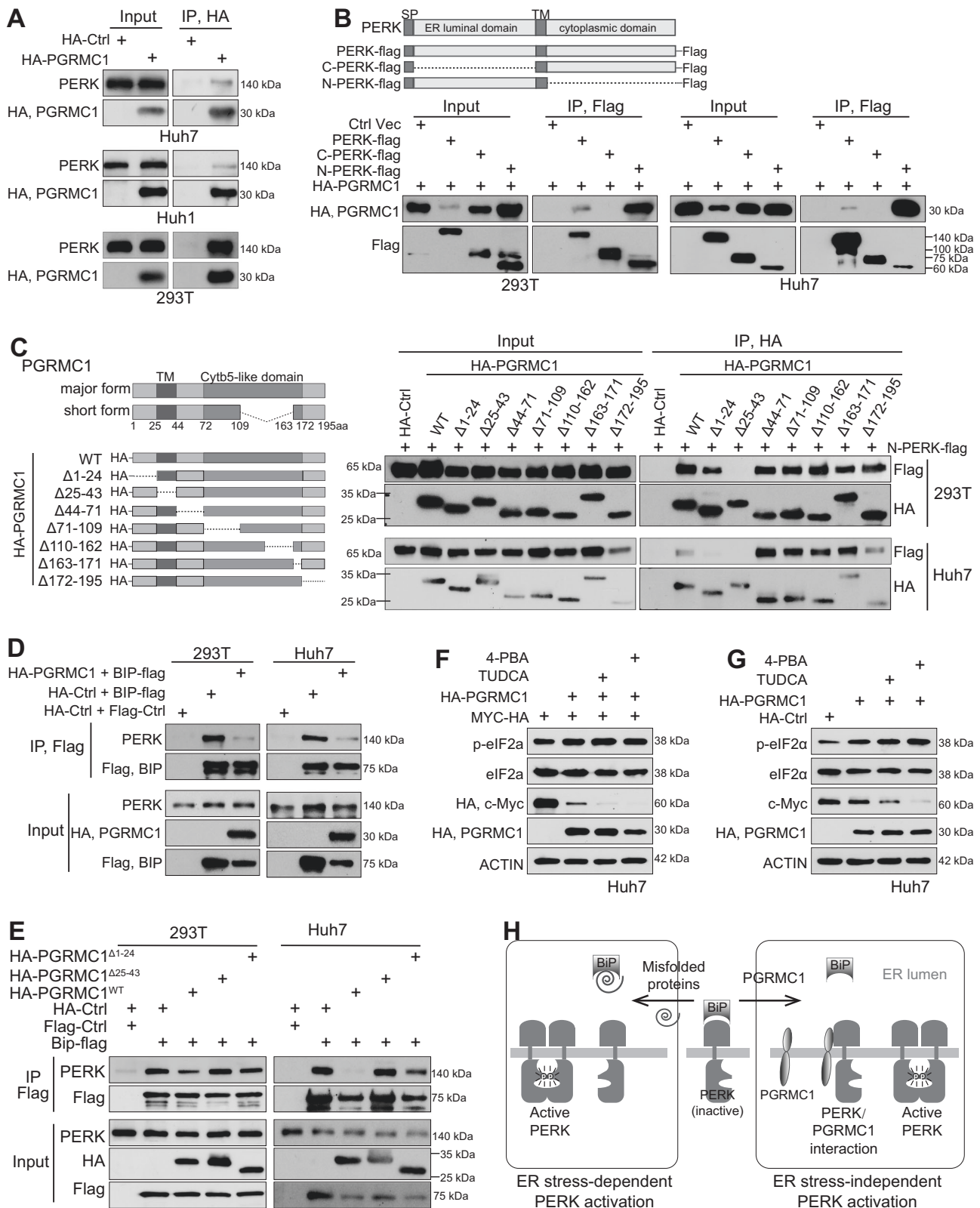


Fig. 4 | PGRMC1 reduced c-Myc protein level by suppressing c-Myc protein translation. The mRNA and protein levels of c-Myc and PGRMC1 in Huh7 and Huh1 cells being transfected with siPGRMC1 **A** or HA-PGRMC1 **B**. Data were from three biological triplicates, and shown as mean \pm standard deviation. **C** Exogenous c-Myc protein level were examined by western blot in Huh7 and Huh1 cells with or without overexpression of PGRMC1. Boncat assay were used for detecting

exogenous **D** and endogenous **E** c-Myc protein translation in Huh7 and Huh1 cells with or without overexpression PGRMC1. **F** Boncat assay were used to detect c-Myc protein translation in Huh7 and Huh1 cells with or without silencing PGRMC1. All these examinations were performed in more than three independent experiments and representative results were shown here. Source data are provided as a Source Data file.





development²¹ and miR-192-5p as a liver-specific miRNA significantly inhibited HCC cancer stem cell features^{22,23}. In this study, we revealed that LSGs were heterogeneously expressed in HCC tumors, and generally downregulated in HCC tumor tissues (Fig. 9). HCC tissues with low LSG expression had poor prognosis and the activated c-Myc signaling. Among all LSGs, 78.3% were non Myc-target genes and HCCs with low expression of these LSGs also possessed a strongly activated

c-Myc pathway. It led to the discovery of LSGs with the capability to suppress c-Myc signaling and the LSG PGRMC1 with the strongest ability in blocking c-Myc-induced orthotopic HCC in vivo. Mechanistically, PGRMC1 promoted ER stress-independent PERK activation via interacting with PERK ER luminal domain, consequently suppressing c-Myc protein translation and blocking c-Myc-induced HCC. Collectively, our findings suggest the important roles of LSGs in c-Myc

Fig. 6 | PGRMC1 interacted with PERK via their ER luminal regions and dis-associated BiP from PERK. **A** Anti-HA IP was performed to detect the interaction of PGRMC1 with PERK in Huh7, Huh1 and 293 T cells when HA-PGRMC1 was transfected. **B** Mapping PERK regions involved in PGRMC1 binding. Anti-flag IPs were performed in 293 T and Huh7 cells co-transfected with HA-PGRMC1 and different PERK-flag vectors. C-PERK, C-terminal region of PERK; N-PERK, N-terminal region of PERK. **C** Mapping PGRMC1 regions involved in PERK binding. Anti-HA IPs were performed in 293 T and Huh7 cells co-transfected with N-PERK-flag and different HA-PGRMC1 vectors. **D** Anti-Flag IP was performed to detect the interaction of BiP and PERK in 293 T and Huh7 cells when BiP-flag was co-transfected with PGRMC1.

E Anti-Flag IP was performed in 293 T and Huh7 cells when BiP-flag was co-transfected with PGRMC1^{WT}, PGRMC1^{Δ25-43} and PGRMC1^{Δ1-24}. **F** Exogenous c-Myc level, p-eIF2α and eIF2α levels in Huh7 cells being transfected with PGRMC1 and with or without TUDCA and 4-PBA treatment. **G** Endogenous c-Myc protein level, p-eIF2α and eIF2α levels in Huh7 cells being transfected with PGRMC1 and with or without TUDCA and 4-PBA treatment. **H** An illustrated model of PGRMC1 activating PERK at an ER stress-independent manner. Immunoblotting images in this figure represent the results from three or more independent experiments. Source data are provided as a Source Data file.

activation in HCC and strategies of restoring PGRMC1 expression might be potentially effective in HCC patients with c-Myc activation (Fig. 9).

In HCC, about 10% of patients present c-Myc amplification while about 30% of patients had c-Myc activation in their tumors²⁴. Here in this study, silencing of LSG PGRMC1 in HCC tumor led to an increased c-Myc protein level. Our previous work revealed that the silencing of LSG CYP39A1 in HCC could increase the transcriptional activity of c-Myc²¹. From our screening methods, several other LSGs such as ABAT and FMO4 suppressed c-Myc-induced HCC too (Fig. 2C, D). In this case, many LSGs might play important roles in suppressing c-Myc signaling. Thus, the reduced expression of LSGs in HCC partially explained a higher rate of c-Myc signaling activation in HCC in comparison with the rate of c-Myc gene amplification (~30% vs. ~10%).

Both classical and non-classical activation models of the ER-located kinase PERK have been reported. In the classical model, unfolded or misfolded proteins cause BiP to be released from PERK, leading to an activation of PERK^{18,37}. In the non-classical model, STING binds and directly activates PERK via their cytoplasmic domains^{20,38}. Here, we further extended the non-classical PERK activation mode. PGRMC1 at the ER interacted with PERK via their ER luminal domains, which also caused BiP to be released from PERK, consequently resulting in PERK activation in an ER stress-independent manner.

Through activating PERK, PGRMC1 inhibited c-Myc protein translation. The significant association between the c-Myc pathway and reduced PGRMC1 levels in HCC was likely due to the c-Myc-mediated hyperactivation of protein synthesis. As a key transcription factor, c-Myc regulates transcription of 10–15% genes in the entire genome. The functions of these genes include ribosome biogenesis, protein synthesis, cell cycle, and metabolism^{39,40}. Therefore, HCC tumors with c-Myc activation would have excessive protein synthesis of c-Myc itself and its downstream targets, and thus could be significantly suppressed by PGRMC1/PERK axis.

The role of PGRMC1 in HCC were rarely reported and only two related publications were found. Dr. Tsai reported the reduced expression of PGRMC1 in HCC tumor tissues and patients with low level of PGRMC1 in their tumor had poor prognosis¹⁶. We presented consistent results with a further large-scale validation using a total of 5 HCC cohorts. Conversely in the other study, Dr. Hong's group reported that patients with high level of PGRMC1 had poor prognosis, and that PGRMC1 KO mice developed slightly less HCC than the control group in a DEN-induced mouse liver tumor model¹⁷. With the in vitro assay they concluded that PGRMC1 KO in macrophages but not hepatocytes contributed to a reduced tumor development in PGRMC1 KO mice via reducing the pro-inflammatory response. In our study, HDTV HCC mouse model was used, in which c-Myc and PGRMC1 were mainly delivered to hepatocytes. HDTV model thus was a relatively ideal model for us to test hepatocyte PGRMC1 in regulating c-Myc-induced HCC. In near future, it will be valuable to continue to investigate macrophage PGRMC1 in regulating c-Myc-induced HCC, as well as hepatocyte PGRMC1 in regulating DEN-induced and other proto-oncogenes-induced HCC. Our preliminary data have found hepatocyte PGRMC1 also suppressed AKT/Ras oncogene induced HCC (Supplementary Fig. 16) so that hepatocyte PGRMC1 might possess an even

broader role in targeting HCC with different genetic background. In addition, hepatocytes played pivotal roles in protein synthesis and PGRMC1 as a LSG activated PERK/p-eIF2α axis. One study also revealed that PGRMC1 attenuated ethanol-induced liver injury⁴¹. It is thus also important to investigate the physiological role of PGRMC1 in hepatocytes.

Investigating the potential of delivering PGRMC1, especially PGRMC1^{1-47aa}, as a therapeutic approach in HCC with c-Myc activation is an intriguing avenue for further research. However, it is also important to approach this with caution. It has been shown that PGRMC1 was upregulated in lung and breast cancer and its upregulation was related to tumor malignant features in cellular based assays¹³⁻¹⁵. In these studies, one key mechanism was that PGRMC1 interacted with EGFR and led to an activated EGFR signaling³⁵. In HCC cells, we have not found such an interaction in cellular and molecular experiments. Considering that these studies mainly included cellular assays or tumor cell line-based xenograft mouse models upon the silencing of PGRMC1, an in-depth investigation with orthotopic cancer mouse models would be meaningful on how PGRMC1 contributed to the development and progress of these cancers. Meanwhile, it would be of great worth to establish the mouse model with lung/breast metastasis of mouse orthotopic HCC and further elucidate whether PGRMC1 contributed to HCC metastasis. Such an investigation will further address the utilization of PGRMC1 or PGRMC1^{1-47aa} in precisely targeting an HCC sub-population with c-Myc activation with/without lung/breast metastasis.

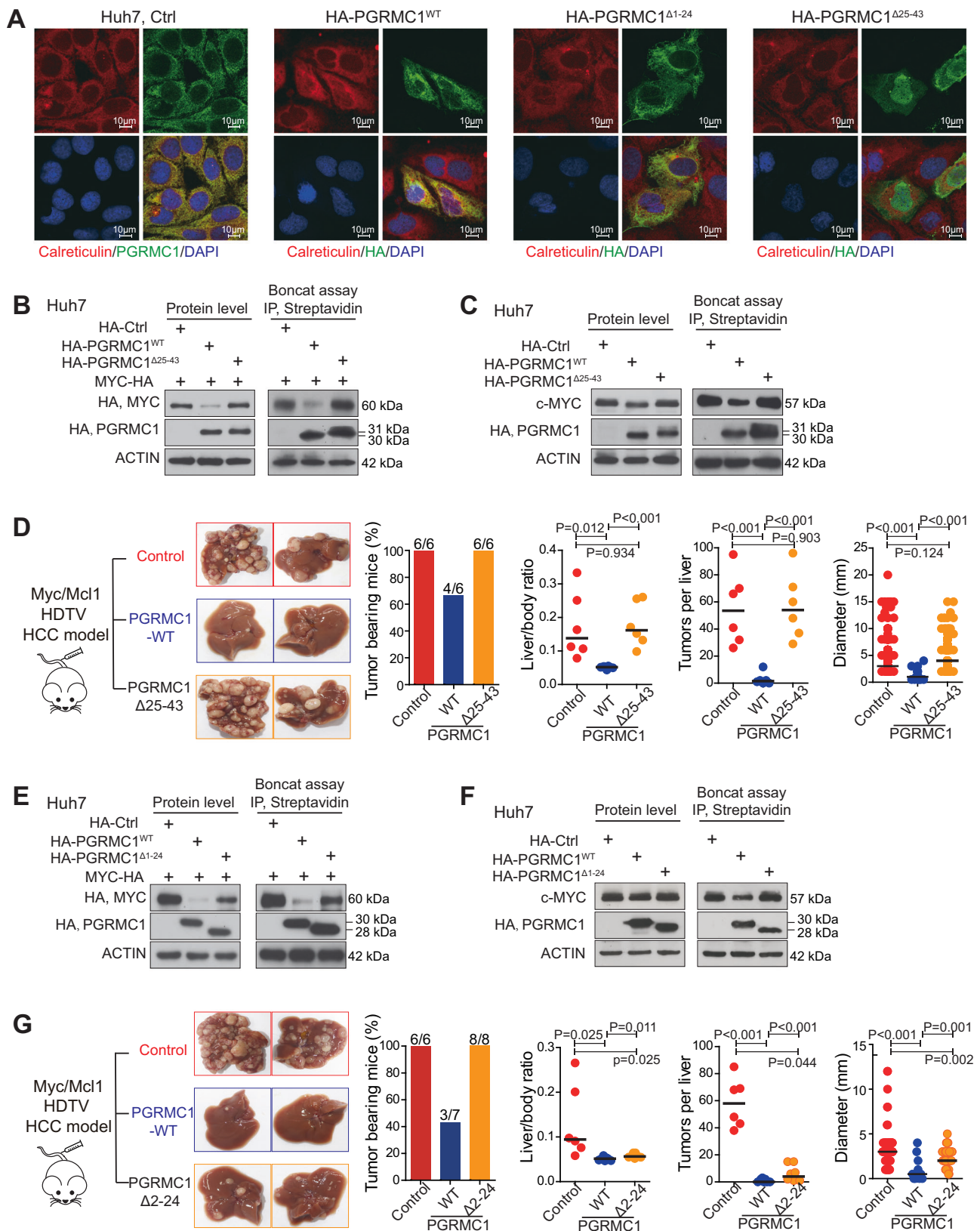
Methods

Approval for work with human subjects and mice was obtained. For human subjects, the study was approved by the institutional review board and ethics committee of Zhejiang Provincial People's Hospital (No.2020QT314) and Sir Run Run Shaw Hospital in Zhejiang University School of Medicine (No.2022-0346). All mouse procedures were conducted under the guidelines and the institutional animal care protocol approved by the Experimental Animal Committee at Zhejiang University (ZJU20200014).

Clinical specimens and databases

A total of five cohorts with a total of 1058 HCC cases were included in this study (Supplementary Table 8).

Cohort 1 included 176 HCC patients. mRNA microarray data (GSE14520) in paired tumor and non-tumor samples were used. Cohort 2 included 371 HCC patients. mRNA sequencing data from 371 tumor tissues and 50 non-tumor liver tissues were used (The Cancer Genome Atlas, <https://portal.gdc.cancer.gov>)²⁴. Cohort 3 included 173 HCC patients. mRNA sequencing data were from 171 paired tumor and non-tumor samples (NHLBI Exome Sequencing Project (ESP); RRID: SCR_012761) and proteomics data were from 159 paired tumor and non-tumor samples⁴². Cohort 4 included 10 HCC patients (5 female and 5 male) from Sir Run Run Shaw Hospital Affiliated to School of Medicine, Zhejiang University, Hangzhou, Zhejiang Province, China. Paired tumor and non-tumor freeze samples were used. The institutional review board and ethics committee of Sir Run Run Shaw Hospital in Zhejiang University School of Medicine approved this study (No.2022-



0346). Cohort 5 included 328 HCC patients from Zhejiang Provincial People's Hospital, Hangzhou, Zhejiang Province, China. 328 tumor tissues and 167 non-tumor liver FFPE tissues were used. The study was approved by the institutional review board and ethics committee of Zhejiang Provincial People's Hospital (No.2020QT314). Informed consent was obtained by participants.

Hydrodynamic injection and mouse monitoring

All mice experiments were approved by the Experimental Animal Committee of Zhejiang University. ICR mice were purchased from Shanghai SLAC Laboratory Animal Co.Ltd. FVB/N mice were from Beijing Vital River Laboratory Animal Technology. All mice were housed in Zhejiang University Laboratory Animal Center in laminar-

Fig. 7 | Both N-terminal domain and ER location of PGRMC1 were vital for PGRMC1 to inhibit c-Myc translation and c-Myc-induced liver tumor formation.

A Confocal microscopy images of PGRMC1 and ER marker Calreticulin and their colocalization in Huh7 cells transfected with HA-Ctrl, HA-PGRMC1^{WT}, HA-PGRMC1^{Δ1-24} and HA-PGRMC1^{Δ25-43}. Scale bar, 10 μm. **B** Boncat assay in Huh7 cells co-transfected with PGRMC1^{WT} or PGRMC1^{Δ25-43} along with MYC-HA. **C** Boncat assay in Huh7 cells transfected with PGRMC1^{WT} or PGRMC1^{Δ25-43}. **D** Liver tumor formation in Myc/Mcl1-induced HCC mouse model with PGRMC1^{WT} or PGRMC1^{Δ25-43} overexpression. Representative images were shown. Liver vs. body ratio, tumor numbers per liver, and tumor diameter were quantified and compared. Six mice per group were used.

Student's t-test was used (two-tailed). **E** Boncat assay in Huh7 cells co-transfected with PGRMC1^{WT} or PGRMC1^{Δ1-24} along with MYC-HA. **F** Boncat assay in Huh7 cells transfected with PGRMC1^{WT} or PGRMC1^{Δ1-24}. **G** Liver tumor formation in Myc/Mcl1-induced HCC mouse model with PGRMC1^{WT} or PGRMC1^{Δ2-24} overexpression. Representative images were shown. Liver vs. body ratio, tumor numbers per liver, and tumor diameter were quantified and compared. Six mice for control group, seven for PGRMC1 group and eight for PGRMC1^{Δ2-24} group were used. Student's t-test was used (two-tailed). Images in panels **A–C** and **E, F** represent the data from three or more independent experiments. Source data are provided as a Source Data file.

flow cabinets under specific pathogen-free conditions at room temperature with a 24-h night-day cycle. All mouse procedures were conducted under the guidelines and the institutional animal care protocol approved by the Experimental Animal Committee at Zhejiang University (ZJU20200014). Based on the protocol, mice will be euthanized when they exhibited any of the following criteria, (1) weight loss, a reduction of more than 20% of their initial body weight; (2) signs of pain or reduced mobility, observable distress, including slower movement, reduced responsiveness to external stimuli, dull or ruffled fur, hunched posture, or inability to access food or water; and (3) behavioral and clinical symptoms including palpable abdominal masses, persistent lethargy, breathing difficulties, or other signs of severe health deterioration. Mice are also euthanized for data collection before the appearance of these syndromes based on the estimated tumor occurrence time or the experimental design.

For oncogene-induced orthotopic HCC tumorigenicity assay, a sleeping beauty (SB) transposon system and four-week-old wild type ICR mice or six-week-old wild-type FVB/N mice was used. Hydrodynamic injection was performed as described. Briefly, oncogenes coding with pT3-EF1α vectors along with pCMV/SB⁴³⁻⁴⁵ was introduced to induce HCC formation through hydrodynamic tail vein (HDTV) injection. pT3-EF1α-PGRMC1, pT3-EF1α-PGRMC1^{Δ2-24}, pT3-EF1α-PGRMC1^{Δ25-43}, pT3-EF1α-PGRMC1^{1-47aa}, pT3-EF1α-ABAT, pT3-EF1α-FMO4, pT3-EF1α-HAGH, pT3-EF1α-SLC10A1 and pT3-U6-shmPerk (mouse Perk) were used to test their functions in regulating HCC formation. For each injection, the combined plasmids were diluted in 2 ml saline (0.9% NaCl), filtered through a 0.22 μm filter, and injected into the lateral tail vein of mice in 5 to 7 s. The detail plasmid combination and amount are listed in Supplementary Table 9. For PGRMC1-mediated HCC suppression in Myc/Mcl1-induced HDTV HCC mouse model, no difference was noticed when using either female or male mice in our initial experiments. In this case, for data consistency only female mice were used in this study. For live mouse bioluminescence imaging assay, at 3 weeks after Myc/Mcl1/Luciferase HDTV injection, FVB/N mice were divided evenly into two groups by bioluminescence signal and injected 1×10¹¹ genomic particles AAV8-TBG-GFP via tail vein, or AAV8-TBG-PGRMC1 respectively. Bioluminescence signals were collected at indicated time point. Mouse survival data were collected. To observe the role of AAV8-TBG-PGRMC1^{1-47aa} in suppressing HCC progression, AAV8-TBG-GFP or AAV8-TBG-PGRMC1^{1-47aa} (1×10¹¹ genomic particles) was used 3 weeks after Myc/Mcl1/Luciferase HDTV injection. Mouse survival data were collected.

Cell Lines, and treatment with cycloheximide (CHX), MG132, Bafilomycin A1 (BafA-1), PERK inhibitor (iPERK), Tunicamycin, Tauroursodeoxycholic Acid (TUDCA) and 4-Phenylbutyric acid (4-PBA)

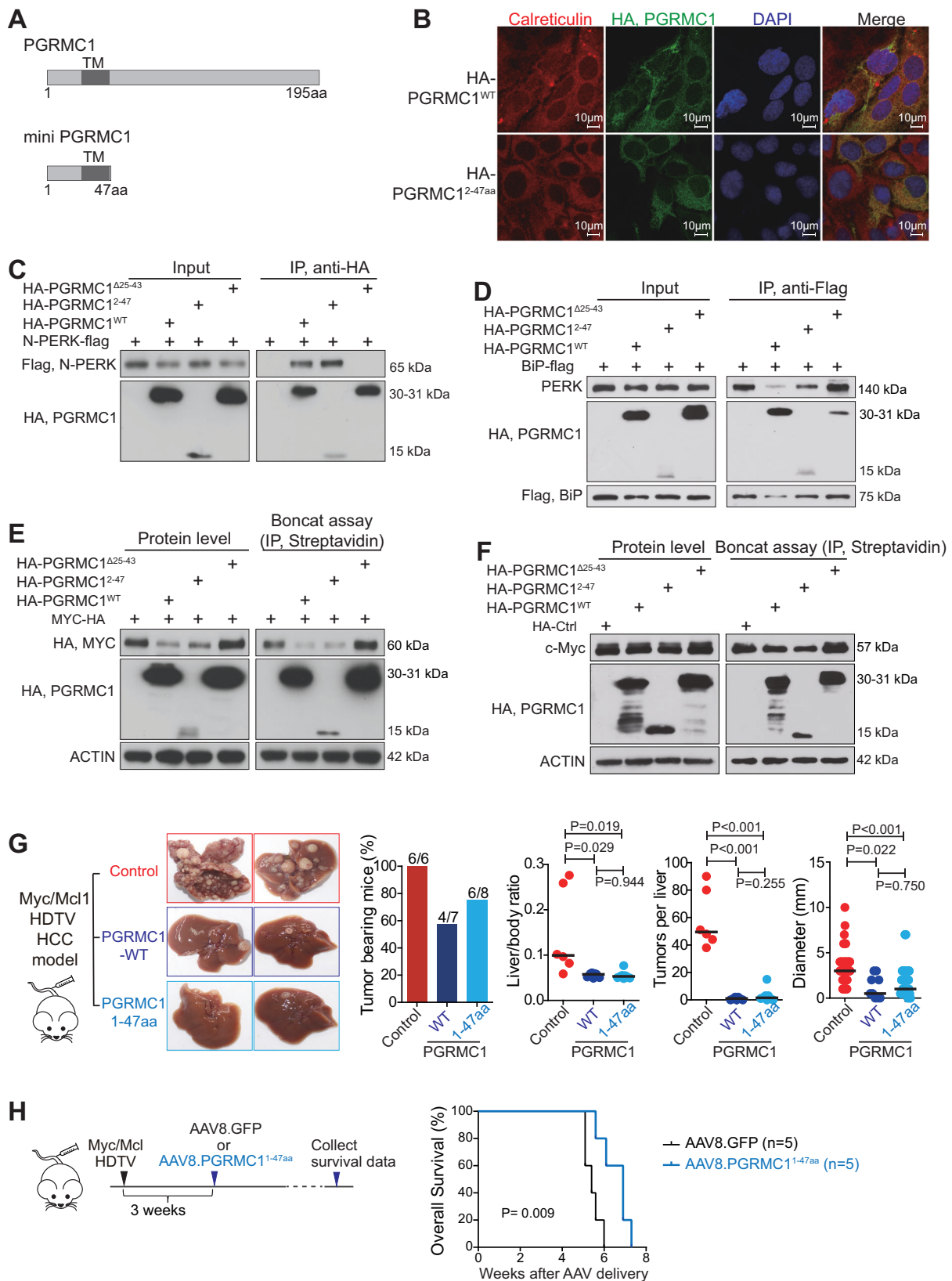
Human HCC cell lines Huh7 and Huh1 were originally from Japanese Collection of Research Biosources Cell Bank (JCRB), and 293 T, NIH3T3 and Hepa1-6 lines were from American Type Culture Collection (ATCC). Briefly, they were maintained in Dulbecco's modified Eagle's medium (DMEM) supplemented with 10% fetal bovine serum, 100 U/

ml penicillin-streptomycin and 1% L-glutamine. No cell lines used in this study were found in the commonly misidentified cell lines maintained by the International Cell Line Authentication Committee (ICLAC) and the NCBI BioSample database. All cells we used in this project were negative for mycoplasma. We routinely examined mycoplasma for our cells once a year, or at any time when we suspected that the cells might be contaminated by mycoplasma. All these cell lines were authenticated via Short Tandem Repeat profile done by GTB Corporation in Suzhou, China.

For CHX assay, cells were treated with 20 μg/ml CHX (Cat#2112, Cell signaling technology) and collected at the indicated time for western blot assay. For MG132 treatment, cells were cultured with 10 μM MG132 (Cat#2194, Cell signaling technology) for the indicated time. For BafA-1 treatment, cells were pretreated with 100 nM BafA-1 (Cat#HY-100558, MedChemExpress) for 4 h, then transfected with indicated plasmids and continually treated with 100 nM BafA-1 for 24 h. Upon the PERK inhibitor treatment, cells were firstly transfected with the indicated plasmid. Four hours after transfection, cells were treated with 10 μM iPERK-1 (GSK2606414, Cat#HY-18072, MedChemExpress) or iPERK-2 (GSK2656157, Cat#HY-13820, MedChemExpress) for 2 h. For tunicamycin, 2 μg/ml tunicamycin (Cat#SC0393, Beyotime Biotechnology) were used to treat cells for the indicated time before cell collection. For TUDCA and 4-PBA, cells were pretreated with 200 μM TUDCA (Cat#S3654, Selleck) or 5 mM 4-PBA (Cat#S3592, Selleck) for 12 h, then transfected the indicated plasmids for 24 h and continually treated with 200 μM TUDCA or 5 mM 4-PBA.

Plasmids and siRNAs, and transfection

Vectors pT3-EF1α-c-Myc (Cat#92046, addgene), pT3-EF1α-MCL1, pT3-EF1α-AKT (Cat#179909, addgene), NRasV12/pT2-CAGGS, pCMV/Sleeping Beauty transposase (pCMV/SB) and pCDNA3.0-MYC-3xHA were originally obtained from Dr. Xin Chen's Lab^{20,21,43-45}. A series of PERK plasmids including p3Xflag-CMV-14-PERK, -PERK^{Δ30-514} and -PERK^{Δ536-1116}, PGRMC1 plasmids including pCDNA3.0-HA-PGRMC1, HA-PGRMC1^{Δ1-24}, HA-PGRMC1^{Δ25-43}, HA-PGRMC1^{Δ44-71}, HA-PGRMC1^{Δ72-109}, HA-PGRMC1^{Δ110-162}, HA-PGRMC1^{Δ163-171}, HA-PGRMC1^{Δ172-195} and HA-PGRMC1^{2-47aa}, as well as plasmids pCDNA3.0-BiP-3xflag, AAV-TBG-PGRMC1, AAV-TBG-PGRMC1^{1-47aa}, pT3-EF1α-PGRMC1^{Δ2-24}, pT3-EF1α-PGRMC1^{Δ25-43}, and pT3-EF1α-PGRMC1^{1-47aa}, were generated via amplifying whole length of PERK, PERK truncations, PGRMC1, PGRMC1 truncations, BiP cDNA fragments through RT-qPCR and inserting them into vectors by restriction enzyme digestion and ligation or homologous recombination (Cat#C113-02, Vazyme). Vectors of pT3-EF1α-PGRMC1, pT3-EF1α-ABAT, pT3-EF1α-FMO4, pT3-EF1α-HAGH, pT3-EF1α-SLC10A1 were generated via recombining PGRMC1, ABAT, FMO4, HAGH and SLC10A1 entry clones with a destination vector pT3-EF1α-attR-ccdb vector using the Gateway LRTM ClonaseTM II Enzyme mix (Cat#11791100, Thermo Fisher Scientific). PLKO.1-shmPERK were constructed via synthesizing shmPERK and inserting it into EcoRI/AgeI sites of PLKO.1 vector. PT3-U6-shCT, PT3-U6-shmPERK #1 and PT3-U6-shmPERK #2 were generated via amplifying whole length of U6-shCT, U6-shmPERK cDNA fragments through RT-qPCR and inserting them into vectors by homologous recombination.



siRNAs for PGRMC1, MYC, EIF2AK1, EIF2AK2, EIF2AK3, and EIF2AK4 as well as negative control siRNA were designed and purchased from GenePharma Co., Shanghai, China.

Lipofectamine 3000 (Cat#L3000015, Invitrogen) reagent was used for transfections of plasmids. Rfect siRNA Transfection Reagent

(Cat# 11011, BIOTRAN) was used for transfections of siRNAs. Lipofectamine 2000 Reagent (Cat# 11668019, Invitrogen) was used for co-transfection of plasmids and siRNAs.

The detailed information for all primers used for constructs and siRNA targeting sequences are listed in Supplementary Data 1.

Fig. 8 | A mini PGRMC1 (1-47aa) interacted with PERK, and reduced c-Myc translation and Myc/Mcl1-induced tumor formation. **A** The diagram of a mini PGRMC1 (47aa), including the N-terminal region and transmembrane domain of PGRMC1. **B** Confocal microscopy images of HA-PGRMC1^{WT} and HA-PGRMC1^{2-47aa} with ER marker Calreticulin and their co-localization in Huh7 cells. **C** Anti-HA IP was performed to detect the interaction of PGRMC1 and PERK in Huh7 cells transfected with HA-PGRMC1^{WT}, HA-PGRMC1^{2-47aa}, or PGRMC1^{Δ25-43}, along with N-PERK-flag. **D** Anti-flag IP was performed to detect the interaction of PERK and BiP in Huh7 cells transfected with BiP-flag together with HA-PGRMC1^{WT}, HA-PGRMC1^{2-47aa}, or PGRMC1^{Δ25-43}. **E** Boncat assay in Huh7 cells co-transfected with MYC-HA along with PGRMC1^{WT}, HA-PGRMC1^{2-47aa}, or PGRMC1^{Δ25-43}. The indicated protein was detected.

F Boncat assay in Huh7 cells transfected with PGRMC1^{WT}, HA-PGRMC1^{2-47aa}, or PGRMC1^{Δ25-43}. **G** Liver tumor formation in Myc/Mcl1-induced HCC mouse model with PGRMC1^{WT} or PGRMC1^{1-47aa} overexpression. Representative images were shown. Liver vs. body ratio, tumor numbers per liver, and tumor diameter were quantified and compared. Six mice for control group, seven for PGRMC1 group and eight for PGRMC1^{1-47aa} group were used. Student's t-test was used (two-tailed). **H** Overall flow of Myc/Mcl1-induced orthotopic HCC mouse model treated with AAV8.GFP or AAV8.PGRMC1^{1-47aa} particle. Five mice per group were used. Overall survival time of mice treated with AAV8 was collected and compared. Log-rank *t* test was performed. Images in panels B-F represent the data from three or more independent experiments. Source data are provided as a Source Data file.

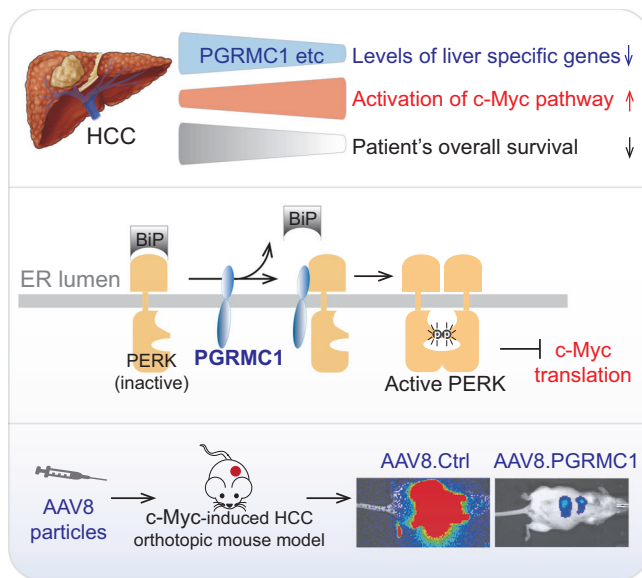


Fig. 9 | Summary of liver specific genes and PGRMC1 in regulating HCC. The deregulated liver-specific genes (LSGs) in HCC were associated with c-Myc oncogenic pathway activation. The LSG PGRMC1 promoted PERK activation in an ER stress-independent manner, and consequently blocked c-Myc-induced hepatic carcinogenesis. Methods restoring the level of liver specific genes such as PGRMC1 hold the potential of treating or even preventing HCC.

Protein extraction, Western blot

Cells were lysed in IP buffer (1% NP40, 150 mM NaCl, 50 mM tris PH 7.4, 10% glycerol) on ice for 30 min, then centrifuged at 13,000 g to separate supernatant fraction. Cell lysates were separated by SDS-PAGE Gel and transferred to PVDF membranes. The membranes were incubated with indicated primary antibodies and then secondary antibodies conjugated to horseradish peroxidase for enhanced chemiluminescence detection of the signals. These antibodies included anti-PGRMC1 (Cat#12990-1-AP, Proteintech, 1:1,000), anti-Flag-M2 (Cat#F3165, Sigma, 1:1,000), anti-c-Myc (Cat#ab32072, Abcam, 1:1,000), anti-HA (Cat#AE008, Abclonal, 1:1,000), anti-PERK (Cat#3192S, CST, 1:1,000), anti-p-PERK (T980, Cat#MA5-15033, Thermo, 1:1,000), anti-eIF2α(S51; Cat#ab32157, Abcam, 1:1,000), anti-p-eIF2α (Cat#ab32157, abcam, 1:1,000), anti-p62 (Cat#66184-1-Ig, Proteintech, 1:1,000), anti-PKR (Cat# 32506, Sigma, 1:1,000), anti-GCN2(Cat# ab134053, Abcam, 1:1,000), anti-IRE1a (Cat#3294 T, CST, 1:1,000), anti-p-IRE1a (Cat#AP1146, Abclonal, 1:1,000), anti-XBP1 (Cat#ab220783, Abcam, 1:1,000), anti-ATF6 (Cat#24169-1-AP, Proteintech, 1:1,000), anti-BiP (Cat#3177 T, CST, 1:1,000), anti-Actin (Cat#AC026, Abclonal, 1:5,000), HRP-linked anti-rabbit IgG antibody (Cat#309-035-003, Jackson Immuno Research, 1:10,000), HRP-linked anti-mouse IgG antibody (Cat#209-035-082, Jackson Immuno Research, 1:10,000).

Boncat assay

In Boncat assay, pulse-labeling is performed. Briefly, cells were firstly cultured with methionine free DMEM (Cat# 21013024, Gibco) for 1 h and then labeled with 50 μM non-canonical amino acid azidohomoalanine (AHA, Cat# 900892, Sigma-Aldrich) for 12 h. The newly synthesized protein carried an active azide (N3) group. Total cells were then lysed with lysis buffer (1%SDS, 50 mM tris pH 8.0) including protease inhibitors and Benzohase endonuclease (Cat# E1014, Sigma-Aldrich). The collected supernatants were incubated with 100 μM alkene-Biotin (Cat# 764213, Sigma-Aldrich) with Click-iT™ Protein Reaction Buffer Kit (Cat# C10276, ThermoFisher). With this click reaction, pulse-labeled newly synthesized proteins were covalently attached to an enrichment biotin tag, purified using Streptavidin-agarose beads (Cat# 20347, Thermo fisher). After washing, the immunoprecipitated proteins were subjected to immunoblotting to examine the newly synthesized proteins.

Immunoprecipitation (IP)

For IP assay, cells were lysed in IP buffer. The supernatants were incubated at 4 °C for overnight with anti-Flag-M2 magnetic beads (Cat# M8823, Sigma) or Pierce™ anti-HA magnetic beads (Cat# 88836, Thermo Scientific). Then, the immunoprecipitated proteins were subjected to immunoblotting.

Associated adenoviruses packaging

Constructs of associated adeno virus AAV-TBG-GFP and AAV-TBG-PGRMC1 were used for AAV packaging with plasmids pHelper (Delta F6 helper) and RepCap (AAV8 serotype packaging plasmid) in 293 T cells. The AAV particles were further purified by iodixanol gradient ultracentrifugation (Cat#, D1556, Millipore) and concentrated by Centrifugal filter (Cat#, UFC9100, Millipore).

Immunohistochemistry (IHC)

For IHC, rabbit polyclonal anti-PGRMC1 (Cat#12990-1-AP, Proteintech, 1:1,000) and Supersensitive enzyme-labeled Goat anti-mouse/Rabbit IgG polymer (Cat#PV-8000, ZSGB-BIO) were used. For each sample, the staining area and intensities were evaluated and graded from 0 to 4 (staining area: 0, 0–5%; 1, 5–25%; 2, 25–50%; 3, 50–75%; 4, >75%) and 0 to 3 (staining intensities: 0, negative; 1, weak; 2, moderate; 3, strong), respectively. A final IHC score between 0 and 12 was achieved by multiplication of staining area and intensity.

Immunofluorescence (IF)

Cells were seeded on coverslips, and then fixed with precooled methanol for 5 min. After being permeabilized with 0.1% Triton X-100 for 10 min, the coverslips were blocked with 3% BSA for 1 h and incubated with primary antibodies at room temperature for 1 h. The cells were then incubated with the corresponding secondary antibodies for 1 h and nuclei were stained with DAPI in the mounting reagent (Cat#E607303, Sangon Biotech, 1 μg/ml). Confocal fluorescence images were captured using a Zeiss LSM 880 AiryScan laser microscope.

These antibodies were PGRMC1 Rabbit Polyclonal Antibody (Cat#I2990-1-AP, Proteintech, 1:1,000), anti-HA Mouse Monoclonal Antibody (Cat#AE008, Abclonal, 1:1,000), and Alexa Fluor® 594 Calreticulin Rabbit Monoclonal antibody (Cat# ab275343, Abcam, 1:500).

RNA extraction and RT-qPCR

Total RNA was isolated using Trizol reagent (Cat#15596018, Invitrogen). cDNA synthesis was performed with 1 µg of total RNA using PrimeScript™ RT reagent Kit with gDNA Eraser (Cat# RR047, Takara). TB Green Premix Ex Taq II (Cat#RR420, Takara) was used for real time PCR (Cat#HSP9655, Bio-rad CFX96). ACTB was used as the reference gene for PGRMC1, EIF2AK1, EIF2AK2, EIF2AK3 and EIF2AK4. All primer sequences are listed in Supplementary Data 1.

Statistical analysis

Hierarchical clustering was performed by the GENESIS software version 1.7.7 developed by Alexander Sturn (IBMT-TUG, Graz, Austria). Gene set enrichment analysis (GSEA) in the Molecular Signatures Database was performed using GSEA V4.2.2. Kaplan–Meier survival analysis was used to compare patient survival and mouse survival among different groups using GraphPad Prism V8.0, and the *P*-value was generated by the Log-Rank test. Class comparison was used for screening for c-Myc related genes. Survival related liver-specific genes were identified by R packages SURVIVAL (V3.3.2). One-way ANOVA, two-way ANOVA, and student's *t*-test (two-side) were used for statistical analysis of comparative data between groups. All *p* values were 2-sided, and *P*-value should be less than 0.05 as significant difference.

Reporting summary

Further information on research design is available in the Nature Portfolio Reporting Summary linked to this article.

Data availability

The mRNA profiling data of cohort 1 used in this study are available in the GEO database of NCBI (GSE14520). The mRNA sequencing data of cohort 2 used in this study are available at the Cancer Genome Atlas (TCGA) portal database (<https://portal.gdc.cancer.gov>). The mRNA transcriptome data and tumor proteome data of cohort 3 are obtained from Dr. Jia Fan⁴². It is also available at <https://www.biosino.org/node/project/detail/OEP000321>. The remaining data are available within the Article, Supplementary Information or Source Data file.

The source data are also provided with this paper including all the “Uncropped blots” and the quantitative data for the graphs. Source data are provided with this paper.

References

- Sung, H. et al. Global Cancer Statistics 2020: GLOBOCAN estimates of incidence and mortality worldwide for 36 cancers in 185 Countries. *CA Cancer J Clin* **71**, 209–249 (2021).
- Kulik, L. & El-Serag, H. B. Epidemiology and management of hepatocellular carcinoma. *Gastroenterology* **156**, 477–491 e471 (2019).
- El-Serag, H. B. Epidemiology of viral hepatitis and hepatocellular carcinoma. *Gastroenterology* **142**, 1264–1273 e1261 (2012).
- Gao, Q. et al. Integrated proteogenomic characterization of HBV-related hepatocellular carcinoma. *Cell* **179**, 1240 (2019).
- Chaisaingmongkol, J. et al. Common molecular subtypes among asian hepatocellular carcinoma and cholangiocarcinoma. *Cancer Cell* **32**, 57–70 e53 (2017).
- Cahill, M. A. Progesterone receptor membrane component 1: an integrative review. *J Steroid Biochem Mol Biol* **105**, 16–36 (2007).
- Peluso, J. J., Liu, X., Gawkowska, A. & Johnston-MacAnanny, E. Progesterone activates a progesterone receptor membrane component 1-dependent mechanism that promotes human granulosa/luteal cell survival but not progesterone secretion. *J Clin Endocrinol Metab* **94**, 2644–2649 (2009).
- Peluso, J. J., Liu, X., Gawkowska, A., Lodde, V. & Wu, C. A. Progesterone inhibits apoptosis in part by PGRMC1-regulated gene expression. *Mol Cell Endocrinol* **320**, 153–161 (2010).
- Peluso, J. J., DeCervo, J. & Lodde, V. Evidence for a genomic mechanism of action for progesterone receptor membrane component-1. *Steroids* **77**, 1007–1012 (2012).
- Mifsud, W. & Bateman, A. Membrane-bound progesterone receptors contain a cytochrome b5-like ligand-binding domain. *Genome Biol* **3**, RESEARCH0068 (2002).
- Hughes, A. L. et al. Dap1/PGRMC1 binds and regulates cytochrome P450 enzymes. *Cell Metab* **5**, 143–149 (2007).
- Oda, S., Nakajima, M., Toyoda, Y., Fukami, T. & Yokoi, T. Progesterone receptor membrane component 1 modulates human cytochrome p450 activities in an isoform-dependent manner. *Drug Metab Dispos* **39**, 2057–2065 (2011).
- Hampton, K. K., Stewart, R., Napier, D., Claudio, P. P. & Craven, R. J. PGRMC1 elevation in multiple cancers and essential role in stem cell survival. *Adv Lung Cancer* **4**, 37–51 (2015).
- Mir, S. U., Ahmed, I. S., Arnold, S. & Craven, R. J. Elevated progesterone receptor membrane component 1/sigma-2 receptor levels in lung tumors and plasma from lung cancer patients. *Int J Cancer* **131**, E1–E9 (2012).
- Asperger, H. et al. Progesterone receptor membrane component 1 regulates lipid homeostasis and drives oncogenic signaling resulting in breast cancer progression. *Breast Cancer Res.* **22**, 75 (2020).
- Tsai, H. W. et al. Progesterone receptor membrane component 1 as a potential prognostic biomarker for hepatocellular carcinoma. *World J Gastroenterol* **24**, 1152–1166 (2018).
- Lee, S. R. et al. Loss of PGRMC1 delays the progression of hepatocellular carcinoma via suppression of pro-inflammatory immune responses. *Cancers* **13**, <https://doi.org/10.3390/cancers13102438> (2021).
- Wang, M. & Kaufman, R. J. Protein misfolding in the endoplasmic reticulum as a conduit to human disease. *Nature* **529**, 326–335 (2016).
- Kopp, M. C., Larburu, N., Durairaj, V., Adams, C. J. & Ali, M. M. U. UPR proteins IRE1 and PERK switch BiP from chaperone to ER stress sensor. *Nat Struct Mol Biol* **26**, 1053–1062 (2019).
- Zhang, D. et al. A non-canonical cGAS-STING-PERK pathway facilitates the translational program critical for senescence and organ fibrosis. *Nat Cell Biol* **24**, 766–782 (2022).
- Ji, F. et al. Blocking hepatocarcinogenesis by a cytochrome P450 family member with female-preferential expression. *Gut* **71**, 2313–2324 (2022).
- Gu, Y. et al. Loss of miR-192-5p initiates a hyperglycolysis and stemness positive feedback in hepatocellular carcinoma. *J Exp Clin Cancer Res.* **39**, 268 (2020).
- Gu, Y. et al. miR-192-5p silencing by genetic aberrations is a key event in hepatocellular carcinomas with cancer stem cell features. *Cancer Res.* **79**, 941–953 (2019).
- Cancer Genome Atlas Research Network, Wheeler, D. A., & Roberts, L. R. Comprehensive and integrative genomic characterization of hepatocellular carcinoma. *Cell* **169**, 1327–1341.e1323 (2017).
- Pope, B. D. et al. Topologically associating domains are stable units of replication-timing regulation. *Nature* **515**, 402–405 (2014).
- Song, L. et al. Open chromatin defined by DNaseI and FAIRE identifies regulatory elements that shape cell-type identity. *Genome Res* **21**, 1757–1767 (2011).
- Dermit, M., Dodel, M. & Mardakheh, F. K. Methods for monitoring and measurement of protein translation in time and space. *Mol Biosyst* **13**, 2477–2488 (2017).
- Dieterich, D. C., Link, A. J., Graumann, J., Tirrell, D. A. & Schuman, E. M. Selective identification of newly synthesized proteins in mammalian cells using bioorthogonal noncanonical amino acid tagging (BONCAT). *Proc Natl Acad Sci USA* **103**, 9482–9487 (2006).

29. Ryu, C. S., Klein, K. & Zanger, U. M. Membrane associated progesterone receptors: promiscuous proteins with pleiotropic functions - focus on interactions with cytochromes P450. *Front Pharmacol* **8**, 159 (2017).
 30. Harding, H. P., Zhang, Y. & Ron, D. Protein translation and folding are coupled by an endoplasmic-reticulum-resident kinase. *Nature* **397**, 271–274 (1999).
 31. Sonenberg, N. & Hinnebusch, A. G. Regulation of translation initiation in eukaryotes: mechanisms and biological targets. *Cell* **136**, 731–745 (2009).
 32. Lee, J. H., Yoon, Y. M. & Lee, S. H. TUDCA-treated mesenchymal stem cells protect against ER stress in the hippocampus of a murine chronic kidney disease model. *Int J Mol Sci* **20**, <https://doi.org/10.3390/ijms20030613> (2019).
 33. Kaur, B. et al. Proteomic profile of 4-PBA treated human neuronal cells during ER stress. *Mol Omics* **14**, 53–63 (2018).
 34. Zheng, P. et al. 4-PBA improves lithium-induced nephrogenic diabetes insipidus by attenuating ER stress. *Am J Physiol Renal Physiol* **311**, F763–F776 (2016).
 35. Kabe, Y. et al. Haem-dependent dimerization of PGRMC1/Sigma-2 receptor facilitates cancer proliferation and chemoresistance. *Nature Commun* **7**, 11030 (2016).
 36. Cahill, M. A. & Medlock, A. E. Thoughts on interactions between PGRMC1 and diverse attested and potential hydrophobic ligands. *J Steroid Biochem Mol Biol* **171**, 11–33 (2017).
 37. Carrara, M., Prischi, F., Nowak, P. R., Kopp, M. C. & Ali, M. M. Non-canonical binding of BiP ATPase domain to Ire1 and Perk is dissociated by unfolded protein CH1 to initiate ER stress signaling. *Elife* **4**, <https://doi.org/10.7554/eLife.03522> (2015).
 38. Sanderson, T. H. et al. PKR-like endoplasmic reticulum kinase (PERK) activation following brain ischemia is independent of unfolded nascent proteins. *Neuroscience* **169**, 1307–1314 (2010).
 39. Dang, C. V. et al. The c-Myc target gene network. *Semin Cancer Biol* **16**, 253–264 (2006).
 40. Dang, C. V. MYC on the path to cancer. *Cell* **149**, 22–35 (2012).
 41. Jo, S. L. et al. Hepatic progesterone receptor membrane component 1 attenuates ethanol-induced liver injury by reducing acetaldehyde production and oxidative stress. *Am J Physiol Gastrointest Liver Physiol* **324**, G442–G451 (2023).
 42. Gao, Q. et al. Integrated proteogenomic characterization of HBV-related hepatocellular carcinoma. *Cell* **179**, 561–577 e522 (2019).
 43. Chow, E. K. H., Fan, L. L., Chen, X. & Bishop, J. M. Oncogene-specific formation of chemoresistant murine hepatic cancer stem cells. *Hepatology* **56**, 1331–1341 (2012).
 44. Mendez-Lucas, A. et al. Glucose catabolism in liver tumors induced by c-MYC can be sustained by various PKM1/PKM2 ratios and pyruvate kinase activities. *Cancer Res.* **77**, 4355–4364 (2017).
 45. Tao, J. et al. Distinct anti-oncogenic effect of various microRNAs in different mouse models of liver cancer. *Oncotarget* **6**, 6977–6988 (2015).
- Central Universities in China (J. Ji), the Joint Research Program of Shaoxing University and Shaoxing Institute, Zhejiang University (2023LHLG001) (J. Ji). S.R. was supported by the German Research Foundation (DFG) project ID 314905040, 469332207 and 493697503 and German Cancer Aid project no. 70113922. J. Jin. was supported by National Natural Science Foundation of China (No. 32470771) and National Key Research and Development Program of China (No. 2022YFC3401500).

Author contributions

J.Ji., and F.J. contributed with conception and design of the work. F.J., J.Z., L.M., Y.T., and Y.Z. contributed with the development of methodology. F.J., J.Z., L.M., Y.T., M.Y., Y.Zhao., J.L., Y.Zhang., and N.Z. executed the experimental work. F.J., X.Z., and J.Ji. performed the analysis and interpretation of data (e.g., statistical analysis, biostatistics, computational analysis). F.J., J.Z., S.R., X.Z., and J.Ji. wrote, review and revised the manuscript. J.S., X.H., J.Y., X.C., B.Z., J.Jin., P.X., and X.Z. provided administrative, technical, or material support. J.Ji. contributed with study supervision. All authors have approved the submitted version.

Competing interests

The authors declare no competing interests.

Additional information

Supplementary information The online version contains supplementary material available at <https://doi.org/10.1038/s41467-024-55745-2>.

Correspondence and requests for materials should be addressed to Junfang Ji.

Peer review information *Nature Communications* thanks the anonymous reviewer(s) for their contribution to the peer review of this work. A peer review file is available.

Reprints and permissions information is available at <http://www.nature.com/reprints>

Publisher's note Springer Nature remains neutral with regard to jurisdictional claims in published maps and institutional affiliations.

Open Access This article is licensed under a Creative Commons Attribution-NonCommercial-NoDerivatives 4.0 International License, which permits any non-commercial use, sharing, distribution and reproduction in any medium or format, as long as you give appropriate credit to the original author(s) and the source, provide a link to the Creative Commons licence, and indicate if you modified the licensed material. You do not have permission under this licence to share adapted material derived from this article or parts of it. The images or other third party material in this article are included in the article's Creative Commons licence, unless indicated otherwise in a credit line to the material. If material is not included in the article's Creative Commons licence and your intended use is not permitted by statutory regulation or exceeds the permitted use, you will need to obtain permission directly from the copyright holder. To view a copy of this licence, visit <http://creativecommons.org/licenses/by-nc-nd/4.0/>.

© The Author(s) 2024

Acknowledgements

We are grateful to our colleagues at the core facility of the Life Sciences Institute for assistance with molecular and cell imaging analysis, and Ms. Julia Zheng for language editing. This work was supported by National Natural Science Foundation of China (82073055 and 82361148723) (J. Ji), the "Pioneer" and "Leading Goose" R&D Program of Zhejiang Province (2023C03052) (J.Ji), National Key R&D Program of China (2018YFA0800504) (J. Ji), the Fundamental Research Funds for the